

# Dissipative superradiant spin amplifier for enhanced quantum sensing

Martin Koppenhöfer<sup>1,\*</sup>, Peter Groszkowski<sup>1</sup>, Hoi-Kwan Lau<sup>2</sup>, and Aashish A. Clerk<sup>1</sup>

<sup>1</sup>*Pritzker School of Molecular Engineering, University of Chicago, Chicago, IL, USA.*

<sup>2</sup>*Department of Physics, Simon Fraser University, Burnaby, BC, Canada.*

(Dated: December 1, 2021)

Quantum metrology protocols exploiting ensembles of  $N$  two-level systems and Ramsey-style measurements are ubiquitous. However, in many cases excess readout noise severely degrades the measurement sensitivity; in particular in sensors based on ensembles of solid-state defect spins. We present a dissipative “spin amplification” protocol that allows one to dramatically improve the sensitivity of such schemes, even in the presence of realistic intrinsic dissipation and noise. Our method is based on exploiting collective (i.e. superradiant) spin decay, an effect that is usually seen as a nuisance because it limits spin-squeezing protocols. We show that our approach can allow a system with a highly imperfect spin-readout to approach SQL-like scaling in  $N$  within a factor of two, without needing to change the actual readout mechanism. Our ideas are compatible with several state-of-the-art experimental platforms where an ensemble of solid-state spins (NV centers, SiV centers) is coupled to a common microwave or mechanical mode.

## I. INTRODUCTION

The field of quantum sensing seeks to use the unique properties of quantum states of light and matter to develop powerful new measurement strategies. Within this broad field, perhaps the most ubiquitous class of sensors are ensembles of two-level systems. Such sensors have been realized in a variety of platforms, including atomic ensembles in cavity QED systems [1–3], and collections of defect spins in semiconductor materials [4–7]. They have also been employed to measure a multitude of diverse sensing targets, ranging from magnetometry [8, 9] to the sensing of electric fields [10] and even temperature [11]. Finding new general strategies for improving such sensors could thus have an extremely wide impact. A general and well-explored method here is to use collective spin-spin interactions to generate entanglement, with the prototypical example being the creation of spin-squeezed states. The intrinsic fluctuations of such states can be parametrically smaller than those of a simple product state [12–14], allowing in principle dramatic improvements in sensitivity. Unfortunately, conventional spin squeezing is only a useful strategy in settings where the extrinsic measurement noise associated with the readout of the spin ensemble is smaller than the intrinsic quantum noise of the ensemble’s quantum state [14, 15]. While this limit of ideal readout can be approached in atomic platforms, typical solid-state spin sensors (such as ensembles of nitrogen vacancy (NV) defect center spins that are read out using spin-dependent fluorescence) have measurement noise that is orders

of magnitude higher than the fundamental intrinsic quantum noise[16].

Spin squeezing ultimately seeks to use entanglement to suppress fundamental spin projection noise. In situations where measurement noise is the key limitation, a potentially more powerful approach is the complementary strategy of *amplification*: before performing readout, increase the magnitude of the “signal” encoded in the spin ensemble. The amplification then effectively reduces the imprecision resulting from any following measurement noise. This strategy is well known in quantum optics [17, 18] and is standard when measuring weak electromagnetic signals. However, it was only recently studied in the spin context [19–25]. Davis *et al.* [19, 22] demonstrated that the same collective spin-spin interaction commonly used for spin squeezing (the so-called one-axis twist (OAT) interaction) could be harnessed for amplification. In the absence of dissipation, they showed that their approach allowed near Heisenberg-limited measurement despite having measurement noise that was on par with the projection noise of an unentangled state. This scheme (which can be viewed as a special kind of more general “interaction-based readout” protocols [24, 26–28]) has been implemented both in cavity QED [3] and in Bose-condensed cold atom systems [29]; a similar strategy was also used to amplify the displacement of a trapped ion [30].

Unfortunately, despite its success in a variety of atomic platforms, the amplification scheme of Ref. [19] is ineffective in setups where the spin ensemble consists of simple two-level systems that experience even small levels of  $T_1$  relaxation (either intrinsic, or due to the cavity mode used to generate collective interactions). As analyzed in the Discussion, the  $T_1$  relaxation both causes a degradation of the signal gain and causes the measurement signal to

---

\* To whom correspondence should be addressed; E-mail: koppenhoefer@uchicago.edu.

be overwhelmed by a large background contribution. This is true even if the single-spin cooperativity is larger than unity. Consequently, this approach to spin amplification cannot be used in many systems of interest, including almost all commonly studied solid-state sensing platforms.

In this work, we introduce a conceptually new spin amplification strategy for an ensemble of  $N$  two-level systems that overcomes the limitation posed by dissipation. Unlike previous work on interaction-based measurement, it does not use collective unitary dynamics for amplification, but instead directly exploits cavity-induced dissipation as the key resource. We show that the collective decay of a spin ensemble coupled to a lossy bosonic mode gives rise to a signal gain  $G$  that exhibits the maximum possible scaling of  $G \propto \sqrt{N}$ . Crucially, in the presence of local dissipation, the amplification in our scheme depends only on the collective cooperativity (not on more restrictive conditions in terms of single-spin cooperativity), and this maximum gain can be reached even in regimes where the single-spin cooperativity is much smaller than unity. Moreover, our amplification mechanism has an “added noise” that approaches the quantum limit one would expect for a bosonic phase-preserving linear amplifier. In addition, the scheme is compatible with standard dynamical decoupling techniques to mitigate inhomogeneous broadening. Finally, unlike existing unitary amplification protocols, which require the signal to be in a certain spin component [19, 22], our scheme amplifies any signal encoded in the transverse polarization of a spin ensemble (similar to phase-preserving amplification in bosonic systems [31]). We stress that in contrast to the majority of interaction-based readout protocols, we are *not* aiming to use entangled states to reach the Heisenberg limit (HL). Instead, our goal is to approach the standard quantum limit (SQL) using conventional dissipative spin ensembles, in systems where extrinsic readout noise is extremely large compared to spin projection noise.

It is interesting to also consider our ideas in a broader context. Our scheme represents a previously unstudied aspect of Dicke superradiance [32–35], a paradigmatic effect in quantum optics. Superradiance is the collective enhancement of the spontaneous emission of  $N$  indistinguishable spins interacting with a common radiation field: if the spins are initialized in the excited state, quantum interference effects will cause a short superradiant emission burst of amplitude  $\propto N^2$  instead of simple exponential decay. In contrast to most work on superradiance, our focus is not on properties of the emitted radiation [32, 36, 37] or optical amplification [38, 39], but rather on the “back-action” on the spin system

itself. This back-action directly generates the amplification effect we exploit. Somewhat surprisingly, we show that our superradiant amplification mechanism continues to be effective in the limit of dissipation-free unitary dynamics, where the collective physics is described by a standard Tavis-Cummings model.

## II. RESULTS

### A. Dissipative gain mechanism and basic sensing protocol

We consider a general sensing setup, where an ensemble of  $N$  two-level systems is subject to a global magnetic field whose value we wish to estimate via a standard Ramsey-type measurement protocol (see Fig. 1(a)). This involves starting the ensemble in a fully polarized coherent spin state (CSS) at time  $t_1$  and letting it rotate under the signal field by an angle  $\phi$ , such that the signal  $\phi$  is encoded in the value of one component of the collective spin vector (here  $\hat{S}_y$ ) at time  $t_2$ . We assume the standard case of an infinitesimal signal  $\phi$ , with  $\langle \hat{S}_y \rangle$  depending linearly on  $\phi$ , and we set  $t_2 = 0$  for convenience. The total error in the estimation of  $\phi$  is then given by (see e.g. [15, 16]):

$$(\Delta\phi)^2 = (\Delta\phi)_{\text{int}}^2 + (\Delta\phi)_{\text{det}}^2 = \frac{(\Delta S_y)^2 + \Sigma_{\text{det}}^2}{|\partial_\phi \langle \hat{S}_y \rangle|^2}, \quad (1)$$

where  $(\Delta S_y)^2 = \langle \hat{S}_y^2 \rangle - \langle \hat{S}_y \rangle^2$ . The first term  $(\Delta\phi)_{\text{int}}^2$  is the intrinsic spin-projection noise associated with the quantum state of the ensemble, while the second term  $(\Delta\phi)_{\text{det}}^2$  describes added noise associated with the imperfect readout of  $\hat{S}_y$ . This additional error can be expressed as an equivalent amount of  $\hat{S}_y$  noise,  $\Sigma_{\text{det}}^2$ , that is referred back to the signal  $\phi$  using the transduction factor  $|\partial_\phi \langle \hat{S}_y \rangle|$ .

Consider first the generic situation where the detection noise completely dominates the intrinsic projection noise,  $(\Delta\phi)_{\text{det}} \gg (\Delta\phi)_{\text{int}}$ . This is the typical scenario in many solid-state systems, e.g. ensembles of NV defects in a diamond crystal whose state is read out using spin-dependent optical fluorescence [16]. The goal is to reduce  $(\Delta\phi)_{\text{det}}$  without changing the final spin readout mechanism (i.e.  $\Sigma_{\text{det}}^2$  remains unchanged). The only option available is “spin amplification”, i.e. enhancement of the transduction factor that encodes the sensitivity of the ensemble to  $\phi$ . Specifically, before doing the final readout of  $\hat{S}_y$ , we want to somehow implement a dynamics that yields

$$\partial_\phi \langle \hat{S}_y(t) \rangle = G(t) \partial_\phi \langle \hat{S}_y(0) \rangle, \quad (2)$$

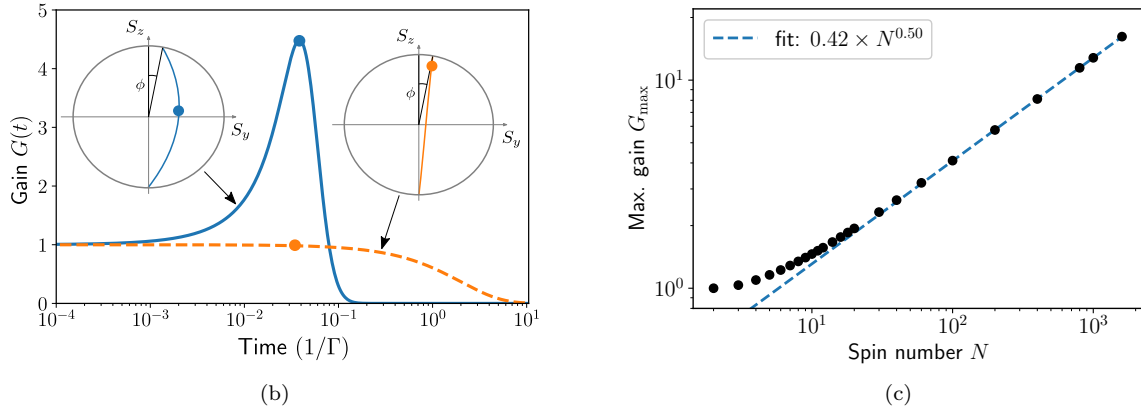
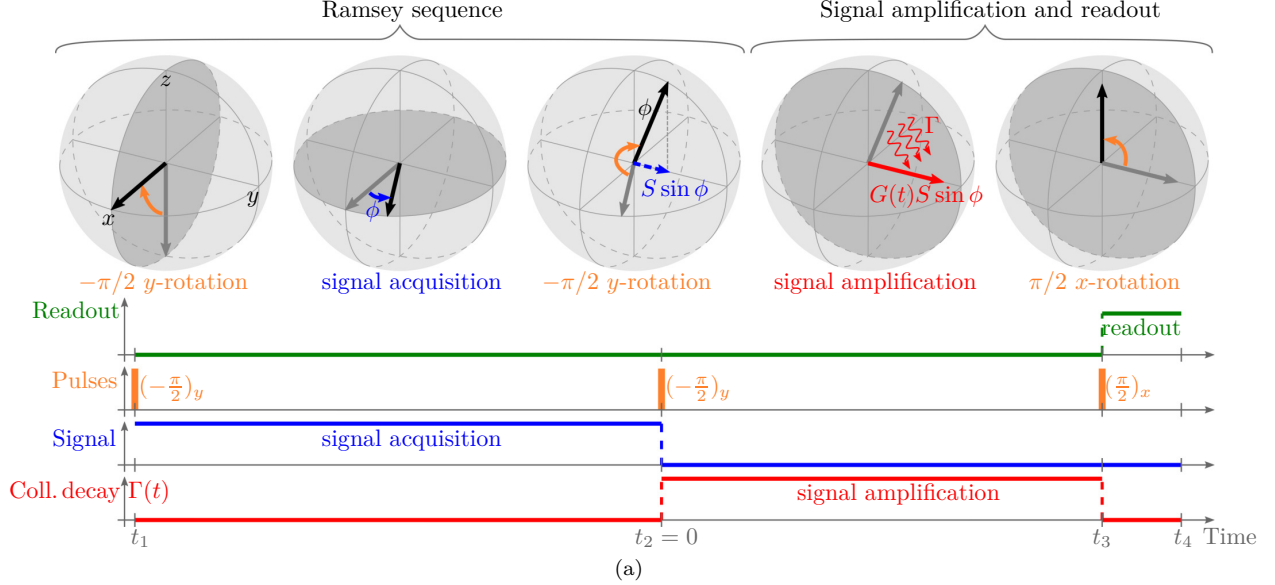


FIG. 1. (a) Schematic showing the superradiant-amplification-enhanced Ramsey measurement protocol: time evolution of the collective spin vector on the Bloch sphere (top row) and corresponding control operations (bottom row). A standard Ramsey sequence encodes a small phase shift  $\phi$  of interest in the  $\hat{S}_y$  spin component. The final state of the Ramsey sequence is chosen to be close to the north pole of the collective Bloch sphere to provide energy for the subsequent amplification step. Collective decay (i.e. the second term in Eq. (3)) leads to passive transient amplification of the signal by a time-dependent gain factor  $G(t)$ . The decay is interrupted at the time of maximum gain and a final  $\pi/2$  rotation maps the amplified signal onto the  $\hat{S}_z$  component for readout. (b) Time-dependent gain  $G(t)$  (defined in Eq. (10)) for collective decay (solid blue curve, numerically exact solution of  $d\hat{\rho}/dt = \Gamma\mathcal{D}[\hat{S}_-]\hat{\rho}$ ) vs. single-spin decay (dashed orange curve,  $d\hat{\rho}/dt = \Gamma\sum_{j=1}^N\mathcal{D}[\hat{\sigma}_-^{(j)}]\hat{\rho}$ ). Only collective decay leads to transient amplification, i.e.  $G(t) > 1$ . We use  $N = 120$  spins and an initial coherent spin state in the  $y$ - $z$ -plane as shown in the third Bloch sphere in (a) with  $\phi = 10^{-5}$ . The insets show sketches of the corresponding trajectories of the spin vector (the initial angle  $\phi$  is exaggerated for readability). (c) Scaling of the maximum gain  $G_{\max}$  with the number  $N$  of spins. Black circles are obtained by full numerical solution of the master equation (3) for  $\gamma_{\text{rel}}/\Gamma = 0$ . The dashed blue line indicates a fit for large  $N$ .

with a time-dependent gain factor  $G(t)$  that is larger than unity at the end of the amplification stage, i.e.  $t = t_3$  in Fig. 1(a). Achieving large gain will clearly reduce the total estimation error in the regime where measurement noise dominates:  $\Delta\phi \rightarrow \Delta\phi/G(t_3)$ . One might worry that in a more gen-

eral situation, where the intrinsic projection noise is also important, this strategy is not useful, as one might end up amplifying the projection noise far more than the signal. We show below that this is not the case for our scheme: even if we use the optimal  $t_3$  which maximizes the gain  $G(t)$ , the amplified

spin-projection noise referred back to  $\phi$  (i.e.  $(\Delta\phi)_{\text{int}}$  in Eq. 1) is only approximately twice the value of this quantity in the initial state. This is reminiscent of the well-known quantum limit for phase-preserving amplification for bosonic systems [17, 31]; we discuss this behaviour in more detail later in the paper.

We next focus on what is perhaps the most crucial issue: how can we implement amplification dynamics in as simple a way as possible? Any kind of amplifier inevitably requires an energy source. Here, this will be achieved by preparing the spin ensemble in an excited state. For concreteness, we assume that the ensemble has a free Hamiltonian  $\hat{H}_0 = \omega\hat{S}_z$ , where  $\omega > 0$  and  $\hbar = 1$ . Hence, at the end of the signal acquisition step at  $t = t_2 = 0$  (see Fig. 1(a)), we rotate the state such that its polarization is almost entirely in the  $+z$  direction (apart from the small rotation caused by the sensing parameter  $\phi$ ), i.e. the ensemble is close to being in its maximally excited state. For the following dynamics, we consider simple relaxation of the ensemble towards the ground state of  $\hat{H}_0$  (where the net polarization is in the  $-z$  direction). Consider now a situation where each spin is subject to independent, single-spin  $T_1$  relaxation (at rate  $\gamma_{\text{rel}}$ ) as well as a collective relaxation process (at rate  $\Gamma$ ). In the rotating frame set by  $\hat{H}_0$ , the Lindblad master equation governing this dynamics is:

$$\frac{d\hat{\rho}}{dt} = \gamma_{\text{rel}} \sum_{j=1}^N \mathcal{D}[\hat{\sigma}_-^{(j)}]\hat{\rho} + \Gamma \mathcal{D}[\hat{S}_-]\hat{\rho}. \quad (3)$$

Here  $\hat{S}_- = \sum_{j=1}^N \hat{\sigma}_-^{(j)}$  is the collective spin-lowering operator,  $\hat{\sigma}_-^{(j)} = (\hat{\sigma}_x^{(j)} - i\hat{\sigma}_y^{(j)})/2$  is the lowering operator of spin  $j$ ,  $\hat{\sigma}_{x,y,z}^{(j)}$  are the Pauli operators acting on spin  $j$ , and  $\mathcal{D}[\hat{O}]\hat{\rho} = \hat{O}\hat{\rho}\hat{O}^\dagger - \{\hat{O}^\dagger\hat{O}, \hat{\rho}\}/2$  is the standard Lindblad dissipation super-operator.

At first glance, it is hard to imagine that such a simple relaxational dynamics will result in anything interesting. Surprisingly, this is not the case. It is straightforward to derive equations of motion that govern the expectation values of  $\hat{S}_x$  and  $\hat{S}_y$ :

$$\frac{d\langle\hat{S}_{x,y}\rangle}{dt} = \frac{\Gamma}{2} \left\langle \left\{ \hat{S}_z, \hat{S}_{x,y} \right\} - \hat{S}_{x,y} \right\rangle - \frac{\gamma_{\text{rel}}}{2} \langle\hat{S}_{x,y}\rangle. \quad (4)$$

Not surprisingly, we see that single-spin relaxation is indeed boring: it simply causes any initial transverse polarization to decay with time. However, the same is not true for the collective dissipation. Within a standard mean-field approximation, the first term on the right-hand side of Eq. (4) suggests that there will be *exponential growth* of both  $\langle\hat{S}_x\rangle$  and  $\langle\hat{S}_y\rangle$  at short times if the condition  $\langle\hat{S}_z\rangle > 1/2$  holds,

i.e. if the spins have a net excitation. This is the amplification mechanism that we will exploit, and that we maximize with our chosen initial condition.

The resulting picture is that with collective decay, the relaxation of the ensemble polarization towards the south pole is accompanied (for intermediate times at least) by a *growth* of the initial values of  $\langle\hat{S}_{x,y}\rangle$ . This ‘‘phase-preserving’’ (i.e. isotropic in the  $S_x$ - $S_y$ -plane) amplification mechanism will generate a gain  $G(t) \geq 1$  that will enhance the subsequent measurement. Numerically-exact simulations show that this general picture is correct, see Fig. 1(b). One finds that the maximum amplification gain  $G(t)$  occurs at a time  $t = t_{\text{max}}$  that approximately coincides with the average polarization vector crossing the equator. We stress that the collective nature of the relaxation is crucial: independent  $T_1$  decay yields no amplification. At a heuristic level, the collective dissipator in Eq. (4) mediates dissipative interactions between different spins, and these interactions are crucial to have gain.

We thus have outlined our basic amplification procedure: prepare a CSS close to the north pole of the generalized Bloch sphere (with  $\phi$  encoded in the small  $\hat{S}_x$  and  $\hat{S}_y$  components of the polarization), then turn on collective relaxation. Stopping the relaxation at time  $t = t_{\text{max}}$  results in the desired amplification of information on  $\phi$  in the average spin polarization; this can be then read out as is standard by converting transverse polarization into population differences via a  $\pi/2$  rotation, as shown in Fig. 1(a). We stress that the generic ingredients needed here are the same as those needed to realize OAT spin squeezing and amplification protocols: a Tavis-Cummings model where the spin ensemble couples to a single, common bosonic mode (a photonic cavity mode [40–42], or even a mechanical mode [43–45]). In previously-proposed OAT protocols, cavity loss limits the effectiveness of the scheme, and one thus works with a large cavity-ensemble detuning to minimize its impact. In contrast, our scheme utilizes the cavity decay as a key resource, allowing one to operate with a resonant cavity-ensemble coupling. In such an implementation, the ability to control the cavity-ensemble detuning provides a means to turn on and off the collective decay  $\Gamma$ . This general setup will be analyzed in more detail below.

Before proceeding to a more quantitative analysis, we pause to note that, for short times and  $\gamma_{\text{rel}} = 0$ , one can directly connect the superradiant spin-amplification physics here to simple phase-preserving bosonic linear amplification. Given our initial state, it is convenient to represent the ensemble using a Holstein-Primakoff bosonic mode  $\hat{a}$  via  $\hat{S}_z \equiv N/2 - \hat{a}^\dagger\hat{a}$ . For short times, one can linearize

the transformation for  $\hat{S}_x$  and  $\hat{S}_y$ , with the result that these are just proportional to the quadratures of  $\hat{a}$ . The same linearization turns the collective decay in Eq. (3) into simple bosonic anti-damping:  $d\hat{\rho}/dt \sim \Gamma N \mathcal{D}[\hat{a}^\dagger]\hat{\rho}$ . This dynamics causes exponential growth of  $\langle \hat{a} \rangle$ , and describes phase-preserving amplification of a non-degenerate parametric amplifier in the limit where the idler mode can be adiabatically eliminated [31]. While this linearized picture provides intuition into the origin of gain, it is not sufficient to fully understand our system: the nonlinearity of the spin system is crucial in determining the non-monotonic behaviour of  $G(t)$  shown in Fig. 1(b), and in determining the maximum gain. We explore this more in what follows.

Finally, we note that Eq. (3) (with  $\gamma_{\text{rel}} = 0$ ) has previously been studied as a spin-only, Markovian description of superradiance, i.e. the collective decay of a collection of two-level atoms coupled to a common radiation field [36, 46]. The vast majority of studies of superradiance focus on the properties of the radiation emitted by an initially excited collection of atoms. We stress that our focus here is very different. We have no interest in this emission (and will not assume any access to the reservoir responsible for the collective spin dissipation). Instead, we use the effective superradiant decay generated by Eq. (3) only as a tool to induce nonlinear collective spin dynamics, which can then be used for amplification and quantum metrology.

### B. Mean-field theory description of superradiant amplification

To gain a more quantitative understanding of our nonlinear amplification process, we analyze the dynamics of Eq. (3) with  $\gamma_{\text{rel}} = 0$  using a standard mean-field theory (MFT) decoupling, as detailed in the Methods. This analysis goes beyond a linearized bosonic theory obtained from a Holstein-Primakoff transformation and is able to capture aspects of the intrinsic nonlinearity of the spin dynamics. We start by using MFT to understand the gain dynamics, which can be determined by considering the evolution of the mean values of the collective spin operator; fluctuations and added-noise physics will be considered later.

As detailed in the Methods, the MFT equation of motion for  $S_z \equiv \langle \hat{S}_z \rangle$  in the large- $N$  limit is

$$\frac{dS_z}{dt} = -\Gamma \frac{N^2}{4} - \Gamma S_z(1 - S_z), \quad (5)$$

where the constant term is obtained by using the fact that the dynamics conserves  $\hat{\mathbf{S}}^2$ . Starting from a highly polarized initial state with  $S_z(0) =$

$N \cos(\phi)/2$ , this equation describes the well-known nonlinear superradiant decay of the  $S_z$  component to the steady state  $|\downarrow\rangle^{\otimes N}$  [37]. The corresponding equations of motion for average values  $S_x$  and  $S_y$  correspond to the expected decoupling of Eq. (4):

$$\frac{dS_{x,y}}{dt} = \Gamma \left( S_z - \frac{1}{2} \right) S_{x,y} \equiv \lambda(t) S_{x,y}, \quad (6)$$

where we have introduced the instantaneous gain rate  $\lambda(t)$ . For  $\lambda(t) > 0$  ( $\lambda(t) < 0$ ), any initial polarization component of the collective average Bloch vector in the  $x$ - $y$  plane will be amplified (damped). Without loss of generality, we chose the initial transverse polarization to be entirely in the  $y$  direction. Thus, the  $S_x$  component will always remain zero since the initial state has  $S_x(0) = 0$ . In contrast, the highly polarized initial state  $S_z(0) \approx N/2 \gg 1/2$  leads to amplification of the nonzero initial value  $S_y(0) = N \sin(\phi)/2$  at short times. In the long run, the superradiant decay evolves  $S_z(t)$  to its steady-state value  $S_z(t \rightarrow \infty) = -N/2$ . As a consequence, for sufficiently long times, the time-dependent gain rate  $\lambda(t)$  will be reduced and amplification ultimately turns into damping if  $S_z(t) < 1/2$ . The MFT equation of motion (17) predicts that maximum amplification of  $S_y$  is achieved at the time  $t_{\text{max}}$  where  $S_z(t_{\text{max}}) = 1/2$ , which is clearly beyond the regime of applicability of a linearized theory based on the Holstein-Primakoff transformation. In the large- $N$  limit, the MFT result for  $t_{\text{max}}$  takes the form

$$t_{\text{max}} = \frac{\ln N}{\Gamma N}, \quad (7)$$

which is the well-known delay time of the superradiant emission peak [37]. The short transient period where  $\lambda(t) > 0$  is enough to yield significant amplification:

$$\begin{aligned} S_{x,y}(t) &= S_{x,y}(0) e^{\int_0^t dt' \lambda(t')} \\ &= S_{x,y}(0) \frac{e^{\Gamma t/2} \cosh\left(\frac{1}{2} \ln N\right)}{\cosh\left(\frac{N}{2} \Gamma t - \frac{1}{2} \ln N\right)}. \end{aligned} \quad (8)$$

Evaluating this at  $t = t_{\text{max}}$  given by Eq. (7) yields the following MFT result for the maximum value of  $S_{x,y}$ :

$$S_{x,y}(t_{\text{max}}) = \frac{\sqrt{N}}{2} S_{x,y}(0). \quad (9)$$

Note that the signal gain *increases* with increasing  $N$  while the waiting time  $t_{\text{max}}$  required to reach the maximum gain *decreases*, giving rise to very fast amplification.

We now verify this intuitive picture derived from MFT using numerically-exact solutions of Eq. (3).

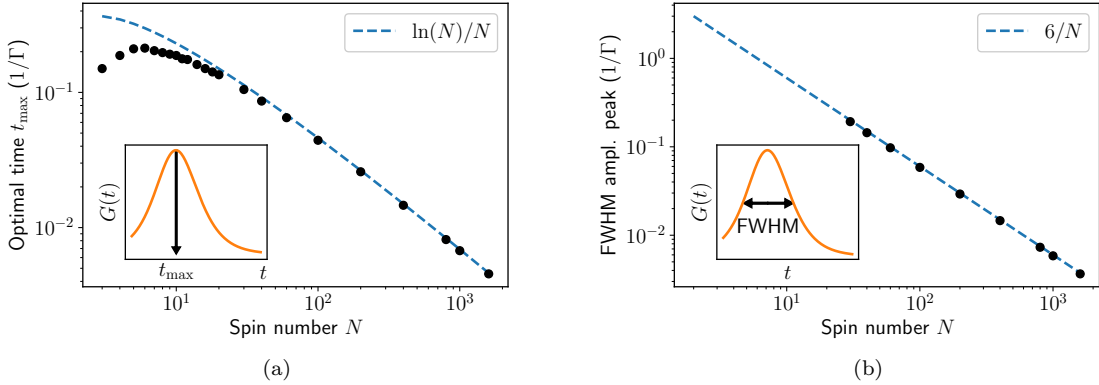


FIG. 2. (a) Optimal time  $t_{\max}$  which maximizes the time-dependent gain  $G(t)$  defined in Eq. (10). (b) Full-width-at-half-maximum of the time-dependent gain  $G(t)$ . In both panels, the black circles have been obtained by a numerically exact solution of the collective relaxation dynamics generated by the master equation (3) for  $\gamma_{\text{rel}}/\Gamma = 0$ . The blue dashed lines indicate fits of the large- $N$  results based on the scaling laws derived using mean-field theory.

To analyze the solutions, we define the time-dependent signal gain  $G(t)$  as follows:

$$G(t) = \lim_{\phi \rightarrow 0} \frac{\langle \hat{S}_y(t) \rangle}{\langle \hat{S}_y(0) \rangle},$$

$$G_{\max} = \max_{t \geq 0} G(t) = G(t_{\max}), \quad (10)$$

where  $t_{\max}$  is determined numerically. Note that this is identical to the definition given in Eq. (2), as  $G(t)$  is independent of  $\phi$  for  $\phi \ll 1$ . Combining Eqs. (9) and (10), we thus expect a scaling  $G_{\max} \propto \sqrt{N}$  based on MFT. Numerically-exact master equation simulations shown in Figs. 1(c) and 2 confirm that (up to numerical prefactors) the scaling of  $G_{\max}$  and  $t_{\max}$  predicted by MFT are correct in the large- $N$  limit.

It is also interesting to note that on general grounds,  $G_{\max} \propto \sqrt{N}$  is the maximal gain scaling that we expect to be possible. This follows from the fact that we would expect initial fluctuations of  $\hat{S}_x$  and  $\hat{S}_y$  to be amplified (at least) the same way as the average values of these quantities, and hence expect  $(\Delta S_x)^2 \geq G_{\max}^2 N/4$ , where  $N/4$  represents the initial fluctuations of  $\hat{S}_x$  in the initial CSS. Next, note that because of the finite dimensional Hilbert space,  $(\Delta S_x)^2$  cannot be arbitrarily large and is bounded by  $N^2/4$ . This immediately tells us that  $G_{\max}$  cannot grow with  $N$  faster than  $\sqrt{N}$ . The gain scaling can also be understood heuristically by using the fact that there is only instantaneous gain for a time  $t < t_{\max} = \ln(N)/N\Gamma$ , and that, during this time period, the instantaneous gain rate is  $\lambda(t) \approx N\Gamma/2$ . Exponentiating the product of this rate and  $t_{\max}$  again yields a  $\sqrt{N}$  scaling.

We stress that the spin-only quantum master

equation (3) as well as the mean-field results for the behaviour of  $S_z$  are well known in the superradiance literature (see e.g. [36, 37, 46]). The new aspect of our work here is to identify the amplification physics associated with superradiant decay, and use MFT to provide a quantitative description of it.

### C. Improving sensitivity and approaching the SQL with extremely bad measurements

We now discuss how the amplification dynamics can improve the total estimation error ( $\Delta\phi$ ) introduced in Eq. (1). For concreteness, we focus on the general situation where the readout mechanism involves adding independent contributions from each spin in the ensemble, and hence the noise associated with the readout itself scales as  $N$ :

$$\Sigma_{\text{det}}^2 \equiv \Xi_{\text{det}}^2 \frac{N}{4}, \quad (11)$$

with  $\Xi_{\text{det}}$  an  $N$ -independent constant. Note that the factor of  $1/4$  in the definition is convenient, as  $\Xi_{\text{det}}^2$  directly describes the ratio of readout noise to the intrinsic projection noise. Equation (11) describes the scaling of readout noise in many practically relevant situations, including standard spin-dependent-fluorescence readout of solid-state spin ensembles [16] and of trapped ions [47]. In this case and for  $\phi \ll 1$ , one has

$$\Xi_{\text{det}}^2 = \frac{1}{\tilde{C}^2 n_{\text{avg}}}, \quad (12)$$

where  $\tilde{C}$  is the fluorescence contrast of the two spin states and  $n_{\text{avg}}$  is the average number of detected

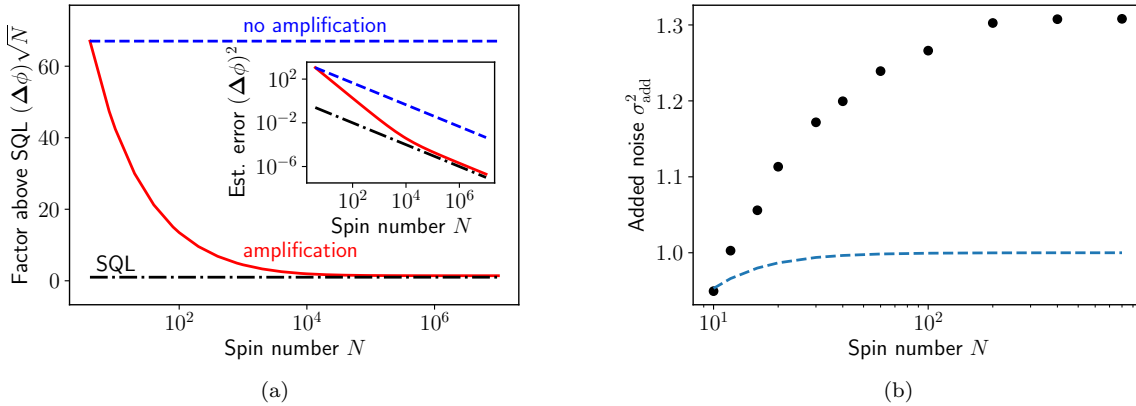


FIG. 3. **(a)** Suppression of detection noise by amplification. The best reported fluorescent readout of an NV ensemble is a factor of  $\Xi_{\text{det}} = 1/\sqrt{\tilde{C}^2 n_{\text{avg}}} = 67$  above the SQL [16]. We assume the ideal case where this factor is independent of the ensemble size (dashed blue line). Amplification suppresses the readout noise (solid red line) and allows one to approach the SQL (dash-dotted black line). The inset shows the scaling of the total estimation error  $(\Delta\phi)^2$  with and without amplification (solid red and dashed blue lines, respectively), and the SQL (dash-dotted black line). The curves have been obtained using a MFT analysis of Eq. (3) for  $\gamma_{\text{rel}}/\Gamma = 0$  and agree qualitatively with numerically exact solutions of the master equation (3), which have been used to calculate the **(b)** added noise  $\sigma_{\text{add}}^2$  (defined in Eq. (14)) for  $\gamma_{\text{rel}}/\Gamma = 0$ . The dash-dotted blue line illustrates the expected minimum amount of added noise,  $1 - 1/G_{\text{max}}^2 N$ , based on a heuristic argument detailed in the Supplemental. Note that this is not a strict lower bound.

photons per spin in a single run of the protocol (see Methods for details).

In considering the estimation error, we will also now account for the fact that our amplification mechanism will not only cause  $\langle \hat{S}_y \rangle$  to grow, but also cause the variance  $(\Delta S_y)^2$  to grow over its initial CSS value of  $N/4$ . The very best case is that the variance is amplified exactly the same way as the signal, but in general there will be excess fluctuations beyond this. This motivates the definition of the *added noise* of our amplification scheme (similar to the definition of the added noise  $\sigma_{\text{add}}$  of a linear amplifier). Letting  $(\Delta \hat{S}_y)^2|_{\text{amp}}$  denote the variance of  $\hat{S}_y$  in the final, post-amplification state of the spin ensemble after an optimal amplification time, we write:

$$(\Delta S_y)^2|_{\text{amp}} \equiv G_{\text{max}}^2 \frac{N}{4} (1 + \sigma_{\text{add}}^2). \quad (13)$$

We have normalized  $\sigma_{\text{add}}$  to the value of the CSS variance; hence,  $\sigma_{\text{add}}^2 = 1$  corresponds to effectively doubling the initial fluctuations (once the gain has been included).

For linear bosonic phase-preserving amplifiers, it is well known that the added noise of a phase-preserving amplifier is at best the size of the vacuum noise [17, 31, 48]. At a fundamental level, this can be attributed to the dynamics amplifying both quadratures of the input signal, quantities that

are described by non-commuting operators. One might expect a similar constraint here, as our spin amplifier also amplifies two non-commuting quantities (namely  $\hat{S}_x$  and  $\hat{S}_y$ ). Hence, one might expect that the best we can achieve in our spin amplifier is to have the added noise satisfy  $\sigma_{\text{add}}^2 = 1$ . A heuristic argument that parallels Caves' classic calculation [17] suggests one indeed has the constraint  $\sigma_{\text{add}}^2 \geq 1 - 1/G^2(T)N$  (see Supplemental). For our system, full master equation simulations let us investigate how the added noise behaves for large  $N$  and maximum amplification. Remarkably, we find  $\sigma_{\text{add}}^2 \approx 1.3$  in the large- $N$  limit, which is just slightly above the expected level based on the heuristic argument (see Fig. 3(b)). This leads to a crucial conclusion: our amplification scheme is useful even if one cares about approaching the SQL.

With the above definitions in hand, we can finally quantify the estimation error in Eq. (1) of our amplification-assisted measurement protocol. Combining Eqs. (2), (11), and (13), one finds that the general expression applied to our scheme reduces to:

$$\begin{aligned} (\Delta\phi)^2 &= \frac{1}{N} \left[ 1 + \sigma_{\text{add}}^2 + \frac{\Xi_{\text{det}}^2}{G_{\text{max}}^2} \right] \\ &= \frac{1}{N} \left[ 1 + \sigma_{\text{add}}^2 + \frac{\Xi_{\text{det}}^2/c_0^2}{N} \right], \end{aligned} \quad (14)$$

where we have used the large- $N$  scaling of the maximum gain in the last equation:  $G_{\text{max}} \propto c_0 \sqrt{N}$  with

$c_0 \approx 0.42$  (see Fig. 1(c)).

There are two crucial things to note here: First, if readout noise completely dominates (despite the amplification), our amplification approach changes the scaling of the estimation error  $(\Delta\phi)^2$  with the number of spins from  $1/N$  to  $1/N^2$ . While this scaling is reminiscent of Heisenberg-limited scaling, there is no connection: in our case, this rapid scaling with  $N$  only holds if one is far from the SQL. Nonetheless, this shows the potential of amplification to dramatically increase sensitivity in this readout-limited regime.

Second, for very large  $N \gg \Xi_{\text{det}}^2$ , the amplification protocol will make the added measurement noise negligible compared to the fundamental noise of the quantum state. In this limit, the total estimation error almost reaches the SQL: it scales as  $(\Delta\phi) \propto \sqrt{(1 + \sigma_{\text{add}}^2)/N} \approx \sqrt{2.3/N}$ . This is only off by a numerical prefactor  $\sqrt{2.3}$  from the exact SQL. We thus have established another key feature of our scheme: using amplification and a large enough ensemble, one can in principle approach the SQL within a factor of two regardless of how bad the spin readout is. For a fixed detector noise  $\Xi_{\text{det}}$ , the crossover in the estimation error from a  $1/N^2$  scaling to a  $1/N$  scaling is illustrated in Fig. 3(a).

#### D. Impact of single-spin dissipation and finite-temperature in the generic model

While our superradiant dissipative spin amplifier exhibits remarkable performance in the ideal case where the only dissipation is the desirable collective loss in Eq. (3), it is also crucial to understand what happens when additional unwanted forms of common dissipation are added.

##### 1. Local dissipation

We first consider the impact of single-spin dissipation, namely Markovian dephasing and relaxation at rates  $\gamma_\phi$  and  $\gamma_{\text{rel}}$ , respectively. The master equation for our spin ensemble now takes the form

$$\begin{aligned} \frac{d\hat{\rho}}{dt} = & \Gamma \mathcal{D}[\hat{S}_-] \hat{\rho} + \gamma_{\text{rel}} \sum_{j=1}^N \mathcal{D}[\hat{\sigma}_-^{(j)}] \hat{\rho} \\ & + \frac{\gamma_\phi}{2} \sum_{j=1}^N \mathcal{D}[\hat{\sigma}_z^{(j)}] \hat{\rho}. \end{aligned} \quad (15)$$

Numerically exact solutions of Eq. (15), shown in Fig. 4, demonstrate that an initial signal is still am-

plified if the collective cooperativities

$$\mathcal{C}_k = \frac{N\Gamma}{\gamma_k}, \quad (16)$$

with  $k \in \{\phi, \text{rel}\}$ , exceed a threshold value of the order of unity. This is equivalent to the threshold condition for superradiant lasing [38, 49]. Further, we find that achieving the maximum gain  $G \propto \sqrt{N}$  does not require strong coupling at the single-spin level: it only requires a large collective cooperativity, and *not* a large single-spin cooperativity  $\mathcal{C}_k/N$ .

Note that the dependence of the gain on cooperativity can be understood at a heuristic level by inspecting the MFT equations of motion (6), which now take the form:

$$\frac{dS_{x,y}}{dt} = \Gamma \left( S_z - \frac{1}{2} \right) S_{x,y} - \gamma_\phi S_{x,y} - \frac{\gamma_{\text{rel}}}{2} S_{x,y}. \quad (17)$$

At short times, the collective decay term tends to increase  $S_y$  at a rate  $N\Gamma$  whereas local dissipation aims to decrease  $S_y$  at rates  $\gamma_\phi$  and  $\gamma_{\text{rel}}/2$ , respectively. Amplification is only possible if the slope of  $S_y$  at  $t = 0$  is positive, which is equivalent to the conditions  $\mathcal{C}_\phi > 1$  and  $\mathcal{C}_{\text{rel}} > 1/2$ , respectively. For weak local dissipation, i.e.  $\mathcal{C}_k \gg 1$ , the numerical results shown in Fig. 4 are well described by the mean-field result

$$G_{\text{max}}(\gamma_k) = G_{\text{max}}(0) \left( 1 - \frac{a_k}{\mathcal{C}_k} \right), \quad (18)$$

where  $a_\phi \approx 3$  and  $a_{\text{rel}} \approx 6$ . In the opposite limit  $\mathcal{C}_k \ll 1$ , there is no amplification,  $G_{\text{max}}(\gamma_k) = 1$ .

##### 2. Finite temperature

Another potential imperfection is that the reservoir responsible for collective relaxation may not be at zero temperature, giving rise to an unwanted collective excitation process. This could be relevant in setups where collective effects stem from coupling to a mechanical degree of freedom, a promising approach for ensembles of defect spins in solids [43–45]. In this general case, the master equation takes the form

$$\frac{d\hat{\rho}}{dt} = \Gamma(n_{\text{th}} + 1) \mathcal{D}[\hat{S}_-] \hat{\rho} + \Gamma n_{\text{th}} \mathcal{D}[\hat{S}_+] \hat{\rho}. \quad (19)$$

The parameter  $n_{\text{th}}$  determines the relative strength between the collective decay and excitation rates and can be interpreted as an effective thermal occupation of the bath generating the collective decay. The gain as a function of the effective thermal



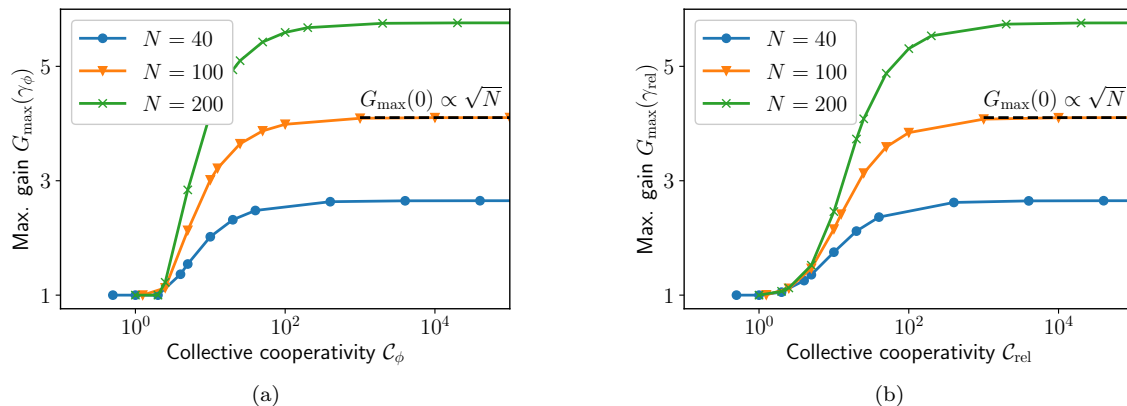


FIG. 4. **(a)** Maximum gain in the presence of local dephasing,  $G_{\max}(\gamma_\phi)$ , as a function of the collective cooperativity  $\mathcal{C}_\phi = N\Gamma/\gamma_\phi$  (calculated by numerically exact integration of the master equation (15) with  $\gamma_{\text{rel}} = 0$ ). Each data point is obtained by maximizing the time-dependent gain  $G(t)$  over the evolution time  $t$ . Collective amplification and local dephasing compete and amplification is observed if  $\mathcal{C}_\phi \gtrsim 2$ , i.e. if the collective amplification rate dominates over local decay. **(b)** Analogous numerical results for maximum gain in the presence of local relaxation,  $G_{\max}(\gamma_{\text{rel}})$ , as a function of the collective cooperativity  $\mathcal{C}_{\text{rel}} = N\Gamma/\gamma_{\text{rel}}$  (with  $\gamma_\phi = 0$ ). We again see that the collective cooperativity is the relevant parameter for obtaining maximum gain.

occupation number  $n_{\text{th}}$  based on numerically exact solution of the full quantum master equation (19) is shown in Fig. 5(a). A nonzero  $n_{\text{th}}$  reduces the gain as compared to the ideal gain  $G_{\max}$  obtained for  $n_{\text{th}} = 0$ , and ultimately prevents any amplification in the limit  $n_{\text{th}} \gg 1$ .

MFT again allows one to develop an intuitive picture of how a bath temperature degrades amplification dynamics. In the presence of finite temperature and for large  $N$ , the mean-field equations of motion (5) and (6) read

$$\frac{dS_{x,y}}{dt} = \Gamma \left( S_z - \frac{1}{2} - n_{\text{th}} \right) S_{x,y}, \quad (20)$$

$$\frac{dS_z}{dt} = -\Gamma \frac{N^2}{4} - \Gamma S_z (1 + 2n_{\text{th}} - S_z). \quad (21)$$

The impact of finite temperature  $n_{\text{th}} > 0$  is thus twofold. First, the time-dependent gain factor in Eq. (20) is shut off at an earlier time, namely, if the condition  $S_z(t) = 1/2 + n_{\text{th}}$  holds. This implies that no amplification will occur if  $n_{\text{th}} > N/2$ . If this were the only effect, the generation of gain would be largely insensitive to thermal occupancies  $n_{\text{th}} \ll N$ . Unfortunately, there is a second, more damaging mechanism. As the above equations show, the instantaneous gain rate  $\lambda(t)$  is controlled by  $S_z(t)$ . The decay of this polarization is seeded by both quantum and thermal fluctuations in the environment. Hence, a non-zero  $n_{\text{th}}$  accelerates this decay, leading to a more rapid decay of polarization, and a shorter time interval where the instantaneous

gain rate is positive. This ultimately suppresses the maximum gain.

The above argument can be made quantitative if we expand  $S_z$  for short times around its initial value,  $S_z = N/2 - \delta$ , where  $\delta \ll 1$ . To leading order in  $N$  and  $\delta$ , the equation of motion of the deviation  $\delta$  is  $d\delta/dt = N\Gamma(1 + n_{\text{th}}) + N\Gamma\delta$ , where the first term shows explicitly that both bath vacuum fluctuations and thermal fluctuations drive the initial decay of polarization. As a consequence, the superradiant emission occurs faster and, in the limit  $N \gg 1 + 2n_{\text{th}}$ , the time to reach maximum amplification is

$$\Gamma t_{\max} = \frac{1}{N} \ln \frac{N - n_{\text{th}}}{n_{\text{th}} + 1}. \quad (22)$$

In the same limit, the maximum gain is given by

$$G_{\max}(n_{\text{th}}) = \frac{G_{\max}(0)}{\sqrt{1 + n_{\text{th}}}}, \quad (23)$$

which shows that a thermal occupation of  $n_{\text{th}} = 3$  will decrease the gain by 3 dB. Note that  $G_{\max}(n_{\text{th}})$  still scales  $\propto \sqrt{N}$ , i.e. for a fixed value of  $n_{\text{th}}$ , the reduction can be compensated by increasing the number of spins.

### E. Implementation using cavity-mediated dissipation

While there are many ways to engineer the collective relaxation that powers our superradiant amplifier, we specialize here to a ubiquitous realization

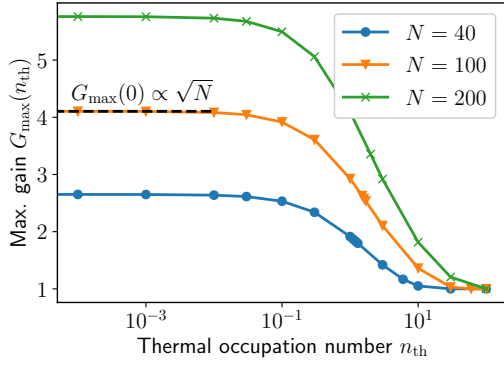


FIG. 5. Maximum gain in the presence of a non-zero thermal occupancy  $n_{\text{th}}$  of the environment responsible for collective spin decay, obtained by numerically exact solution of the master equation (19). Each data point is obtained by maximizing the gain  $G(t)$  over the evolution time  $t$ . We see that a non-zero bath thermal occupancy rapidly degrades gain. At a heuristic level, the decay of the ensemble's  $z$  polarization is seeded by both thermal and quantum bath fluctuations. Non-zero thermal fluctuations hence accelerate the decay, leading to a shorter time interval where the instantaneous gain rate  $\lambda(t)$  is positive. This allows one to quantitatively understand the suppression of maximum gain seen here, see Eq. (23).

that allows the tuneability we require: couple the spin ensemble to a common lossy bosonic mode. To that end, we consider a setup where  $N$  spin-1/2 systems are coupled to a damped bosonic mode  $\hat{a}$  by a standard Tavis-Cummings coupling (see Fig. 6):

$$\hat{H} = \omega_{\text{cav}} \hat{a}^\dagger \hat{a} + \sum_{j=1}^N \omega_j \frac{\hat{\sigma}_z^{(j)}}{2} + \sum_{j=1}^N g_j \left( \hat{\sigma}_-^{(j)} \hat{a}^\dagger + \hat{\sigma}_+^{(j)} \hat{a} \right). \quad (24)$$

Here,  $\omega_{\text{cav}}$  and  $\omega_j$  denote the frequencies of the bosonic mode and the spins, respectively, and  $g_j$  denotes the coupling strength of spin  $j$  to the bosonic mode. The bosonic mode is damped at an energy decay rate  $\kappa$  and the entire system is thus described by the quantum master equation

$$\frac{d\hat{\rho}}{dt} = -i [\hat{H}, \hat{\rho}] + \kappa \mathcal{D}[\hat{a}] \hat{\rho}. \quad (25)$$

For collective phenomena, we ideally want all atoms to have the same frequency  $\omega_j = \bar{\omega}$  and be equally coupled to the cavity,  $g_j = g$ . For superradiant decay, we further want the spins to be resonant with the cavity, i.e. have zero detuning  $\omega_{\text{cav}} - \bar{\omega} = 0$ . If, in addition, the bosonic mode is strongly damped,  $\kappa \gg \sqrt{N}g$ , the  $\hat{a}$  mode can be eliminated adiabatically, which gives rise to the spin-only master equation

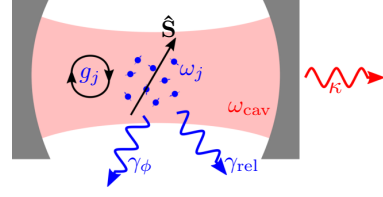


FIG. 6. The collective decay described by Eqs. (3) and (15) can be implemented experimentally by coupling  $N$  spin-1/2 systems (level splittings  $\omega_j$ ) to a strongly damped bosonic mode (frequency  $\omega_{\text{cav}}$  and single-spin coupling strengths  $g_j$ ). The mode is depicted here as a resonant mode of a photonic cavity, but one could use a wide variety of systems (e.g. microwave or mechanical modes). The energy decay rate of the bosonic mode is  $\kappa$  and each spin may undergo local relaxation or dephasing processes at rates  $\gamma_{\text{rel}}$  or  $\gamma_{\phi}$ , respectively.

tion (3) with a collective decay rate

$$\Gamma = \frac{4g^2}{\kappa} \quad (26)$$

and  $\gamma_{\text{rel}} = 0$ .

Returning to Fig. 1, note that a crucial part of our protocol is the ability to turn on and off the collective dissipation on demand (i.e. to start the amplification dynamics at the appropriate point in the measurement sequence, and then turn it off once maximum gain is reached). This implementation provides a variety of means for doing this. Perhaps the simplest is to control the spin-cavity detuning  $\Delta$  by, e.g. changing the applied  $z$  magnetic field on the spins. In the limit of an extremely large detuning, the superradiant decay rate  $\Gamma$  is suppressed compared to Eq. (26) by the small factor  $\kappa^2/(\kappa^2 + 4\Delta^2) \ll 1$ .

In the following, we separately analyze the impact of coupling inhomogeneities,  $g_j \neq g$ , and of inhomogeneous broadening,  $\omega_j \neq \bar{\omega}$ .

### 1. Non-uniform single-spin couplings

To analyze the impact of inhomogeneous coupling parameters  $g_j$ , we follow the standard approach outlined in Ref. [36]. It uses an expansion of the mean-field equations to leading order in the deviations  $\delta_j = g_j - \bar{g}$  of the average coupling  $\bar{g} = \sum_{j=1}^N g_j/N$  and retains only leading-order terms in the equations of motion for  $S_x$  and  $S_y$ . The impact of inhomogeneous couplings is then to reduce the effective length of the collective spin vector associated with the ensemble by the factor

$$\mu = \frac{1}{N} \frac{\sum_{k=1}^N \sum_{l=1, l \neq k}^N g_k g_l}{\sum_{k=1}^N g_k^2}, \quad (27)$$

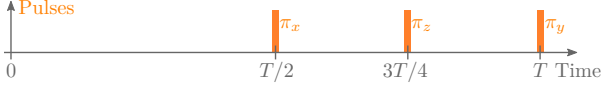


FIG. 7. Dynamical decoupling sequence to cancel inhomogeneous broadening in the Hamiltonian (24). The  $\pi$  pulse about the  $x$  axis cancels disorder in the spin frequencies  $\omega_j$ . The subsequent  $\pi$  pulses about the  $z$  and  $y$  axis compensate unwanted interaction terms generated by the first  $\pi$  pulse. The overall pulse sequence is applied repeatedly and generates the average Hamiltonian (28) if the repetition rate  $1/T$  is much larger than the standard deviation of the distribution of the spin transition frequencies  $\omega_j$ .

i.e. the maximum gain and the optimal time are now given by  $G_{\text{ci}} = \sqrt{\mu N}/2$  and  $t_{\text{max}}^{\text{ci}} = \ln(\mu N)/\gamma_0 \mu N$ , respectively, where we defined  $\gamma_0 = \sum_{k=1}^N 4g_k^2/\kappa N$ . Hence, the maximum gain  $G_{\text{max}}$  is reduced by a disorder-dependent prefactor, but the fundamental scaling is retained.

### 2. Inhomogeneous broadening

Inhomogeneous broadening can be canceled by the dynamical decoupling sequence introduced recently in Ref. [50], which is summarized in Fig. 7. Different spin transition frequencies  $\omega_j$  in Eq. (24) lead to a dephasing of the individual spins in the ensemble, which can be compensated by a  $\pi$  pulse about the  $x$  axis halfway through the sequence. However, this pulse will modify the interaction term in Eq. (24) and will turn collective decay into collective excitation. This can be compensated by a  $\pi$  pulse about the  $z$  axis at time  $3T/4$ , which changes the sign of the coupling constants  $g_j$ . Note that such a pulse can be generated using a combination of  $x$  and  $y$  rotations. The final  $\pi$  pulse about the  $y$  axis at time  $T$  reverts all previous operations and restores the original Hamiltonian (24). The average Hamiltonian of this pulse sequence in a frame rotating at  $\omega_0$  is

$$\bar{H} = \sum_{j=1}^N \frac{g_j}{2} \left( \hat{\sigma}_+^{(j)} \hat{a} + \hat{\sigma}_-^{(j)} \hat{a}^\dagger \right) \quad (28)$$

if the repetition rate  $1/T$  of the decoupling sequence is much larger than the standard deviation of the distribution of the frequencies  $\omega_j$ . More details on the derivation of this decoupling sequence are provided in a recent preprint [50].

### 3. Limit of an undamped cavity

Returning to our cavity-based implementation of the superradiant spin amplifier in Eqs. (24) and (25), one might worry about whether this physics also persists in regime where the cavity damping rate  $\kappa$  is not large enough to allow for an adiabatic elimination. To address this, we briefly consider the extreme limit of this situation,  $\kappa \rightarrow 0$ , where we simply obtain a completely unitary dynamics generated by the resonant Tavis-Cummings Hamiltonian

$$\hat{H}_{\text{TC}} = \omega_{\text{cav}} \hat{a}^\dagger \hat{a} + \omega \hat{S}_z + g \left( \hat{S}_- \hat{a}^\dagger + \hat{S}_+ \hat{a} \right), \quad (29)$$

where  $\omega_{\text{cav}} = \omega$ . Figure 8 shows numerical results for the time-maximized gain  $G_{\text{max}}$  starting from an initial state  $e^{i\phi \hat{S}_x} |\uparrow \dots \uparrow\rangle \otimes |0\rangle$ , where  $|0\rangle$  denotes the vacuum state of the cavity. A complementing analysis based on MFT is discussed in the Supplemental. We find that spin amplification dynamics still holds in the unitary regime, with an identical  $G_{\text{max}} \propto \sqrt{N}$  scaling of the maximum gain. We stress that realizing this limit of fully unitary collective dynamics is challenging in most spin ensemble sensing platforms. Nonetheless, this limit shows that our amplification dynamics will survive even if the adiabatic elimination condition  $\sqrt{N}g \ll \kappa$  that leads to Eq. (25) is not perfectly satisfied. This further enhances the experimental flexibility of our scheme.

Although both the dissipative and the unitary case yield  $G_{\text{max}} \propto \sqrt{N}$ , the underlying dynamics is quite different. The time  $t_{\text{max}}$  to reach maximum amplification in the coherent case, shown in Fig. 8(a), is parametrically longer if we consider the limit of a large number of spins  $N$ :  $t_{\text{max}} \propto \ln \sqrt{N}/\sqrt{N}$  (as opposed to a  $t_{\text{max}} \propto \ln N/N$  scaling in the dissipative case). Consequently, the instantaneous gain rates  $\lambda(t)$  are also quite different in both cases: whereas dissipative superradiant decay has an almost constant instantaneous gain rate over a very short time, the gain in the Tavis-Cummings model is non-monotonic, starts at zero, and grows at short times, as shown in Fig. 8(b).

Note that, for the coherent Tavis-Cummings model, the timescale for maximum amplification is analogous to the timescale that governs quasi-periodic oscillations of excitation number in the large- $N$  limit; this latter phenomenon has been derived analytically in previous work [51–53]. However, the semiclassical approach used in these works fails to accurately describe the gain physics that is of interest here (see Supplemental). Finally, in the Supplemental, we show that the added noise in the unitary case is also close to the expected quantum limit. Surprisingly, it is approximately equal to what we have found in the dissipative limit,  $\sigma_{\text{add}}^2 \approx 1.3$ .

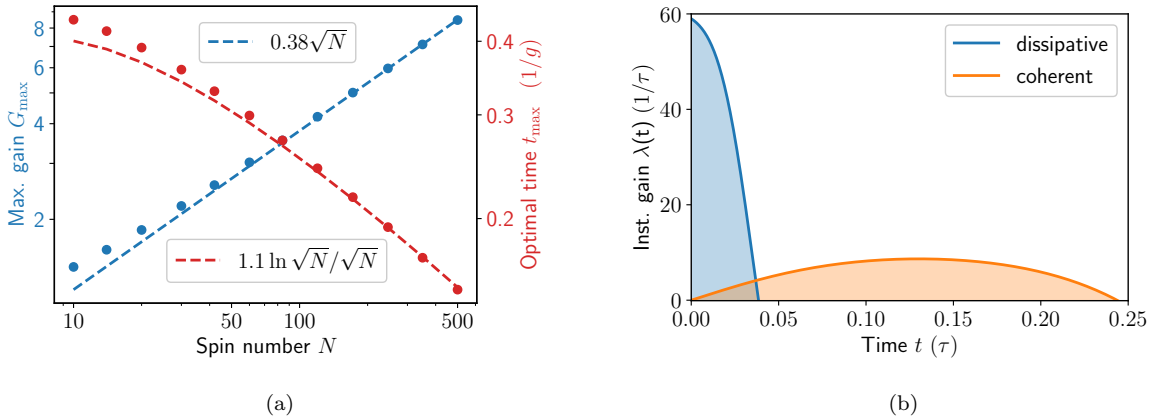


FIG. 8. Coherent spin amplification in a cavity-spin system described by the resonant Tavis-Cummings Hamiltonian (29) with  $\omega_{\text{cav}} = \omega$  and initial state  $e^{i\phi\hat{S}_x} |\uparrow \dots \uparrow\rangle \otimes |0\rangle$ . (a) The maximum gain  $G_{\max}$  follows the same  $\sqrt{N}$  scaling as in the dissipative case, while the optimal evolution time  $t_{\max} \propto \ln \sqrt{N} / \sqrt{N}$ , has a different  $N$ -dependence than the corresponding time  $t_{\max} \propto \ln N / N$  in the dissipative case (cf. Fig. 2(a)). Colored dots correspond to data obtained from solving the Schrödinger equation, while the dashed curves show the corresponding large- $N$  scaling behavior. (b) Comparison of the instantaneous gain  $\lambda(t) = [d\langle \hat{S}_y(t) \rangle / dt] / \langle \hat{S}_y(t) \rangle$  as a function of time for coherent (orange) and dissipative (blue) amplification protocols with  $N = 120$  spins. The time scale  $\tau$  (which is  $N$ -independent) is  $1/g$  and  $1/\Gamma$  for the coherent and dissipative cases, respectively. The maximum gain  $G_{\max}$  shown in (a) corresponds to the integral of  $\lambda(t)$  between  $t = 0$  and  $t = t_{\max}$  (i.e. the shaded regions), which are nearly equal in both cases. All numerical results presented here for the unitary scheme are obtained by numerical integration of the Schrödinger equation with Hamiltonian (29).

### III. DISCUSSION

#### A. Comparison and advantages over unitary OAT amplification schemes

The dissipative spin amplification scheme introduced in this work is effective in the presence of collective loss, and in fact harnesses this as a key resource. As discussed in the introduction, this is in sharp contrast to conventional approaches that use unitary dynamics to improve sensing in the presence of measurement noise: such approaches become infeasible with even small amounts of  $T_1$  relaxation (whether collective or single-spin in nature). To illustrate this, we focus on the scheme presented in the seminal work by Davis *et al.* [19], where OAT dynamics is used to generate effective spin amplification. This scheme involves starting a spin ensemble in a CSS  $|\psi_0\rangle$  that is fully polarized in the  $x$  direction. The protocol then corresponds to the composite unitary evolution

$$|\psi_f\rangle = \hat{U}_{\text{amp}} \hat{R}_y(\phi) \hat{U}_{\text{sqz}} |\psi_0\rangle. \quad (30)$$

The first step corresponds to the generation of squeezing using the OAT Hamiltonian  $\hat{H}_{\text{OAT}} = \chi \hat{S}_z^2$  for a time  $t$ , i.e.  $\hat{U}_{\text{sqz}} = \exp(-i\hat{H}_{\text{OAT}}t)$ . The next step is signal acquisition: the state is rotated by

a small angle  $\phi$  about the  $\hat{S}_y$  axis, via the unitary  $\hat{R}_y(\phi) = e^{-i\phi\hat{S}_y}$ . Finally, the last step is another evolution under the OAT interaction Hamiltonian, for an identical time  $t$  as the first step, but with an opposite sign of the interaction  $\chi \rightarrow -\chi$ , i.e.  $\hat{U}_{\text{amp}} = \hat{U}_{\text{sqz}}^{-1}$ .

In this scheme, the final signal gain is created entirely by the last OAT evolution step  $\hat{U}_{\text{amp}}$ ; the first “pre-squeezing” step only serves to control the fluctuations in the final state. As the primary focus here is on the gain (and on regimes where extrinsic readout noise dominates over projection noise), we can ignore the initial squeezing step. We thus consider a CSS that is almost completely polarized in the  $x$  direction, with a small  $z$  polarization that encodes the signal rotation  $\phi$  of interest. Without dissipation, the OAT Hamiltonian leads to the Heisenberg equation of motion:

$$\frac{d\hat{S}_y}{dt} = 2\chi\hat{S}_z\hat{S}_x. \quad (31)$$

For short times, we have  $S_x \approx N/2$ , and the OAT interaction causes the expectation value of  $S_y$  to grow linearly in time at a rate set by the initial “signal” value of  $S_z = N \sin(\phi)/2$ . The amplified signal is thus contained in  $S_y$ , and it is this spin component that is ultimately read out. We can thus define the

signal gain analogously as in Eq. (10),

$$G^{\text{OAT}}(t) \equiv \lim_{\phi \rightarrow 0} \frac{\langle \hat{S}_y(t) \rangle}{\langle \hat{S}_z(0) \rangle}. \quad (32)$$

Note that the amplification mechanism here is analogous to bosonic amplification using a QND interaction [54, 55]. In the spin system, nonlinearity eventually causes the the growth of  $S_y$  to saturate, leading to a maximum gain at a time  $t_{\text{max}}^{\text{OAT}} \propto 1/\chi\sqrt{N}$  [19].

A crucial aspect of the OAT gain-generation mechanism is the conservation of  $\hat{S}_z$  (analogous to a QND structure in the bosonic system). This leaves it vulnerable to any unwanted dissipative dynamics that breaks this conservation law. Unfortunately, such symmetry breaking is common in many standard sensing setups. Consider perhaps the simplest method for realizing an OAT Hamiltonian, where the spin ensemble is coupled to a bosonic mode (e.g. a photonic cavity mode or mechanical mode) via the Tavis-Cummings Hamiltonian (29). Working in the large detuning limit  $|\Delta| = |\omega_{\text{cav}} - \omega| \gg g$  allows one to adiabatically eliminate the bosonic mode. This results in both the desired OAT Hamiltonian interaction, but also a collective loss dissipator associated with the loss rate  $\kappa$  of the cavity mode:

$$\begin{aligned} \frac{d\hat{\rho}}{dt} = & -i \left[ \chi \hat{S}_z^2, \hat{\rho} \right] + \Gamma_{\text{coll}} \mathcal{D}[\hat{S}_-] \hat{\rho} \\ & + \gamma_{\text{rel}} \sum_{j=1}^N \mathcal{D}[\hat{\sigma}_-^{(j)}] \hat{\rho} + \frac{\gamma_{\phi}}{2} \sum_{j=1}^N \mathcal{D}[\hat{\sigma}_z^{(j)}] \hat{\rho}, \end{aligned} \quad (33)$$

where the OAT strength is  $\chi = g^2/\Delta$  and the collective decay rate is  $\Gamma_{\text{coll}} = \chi\kappa/\Delta$ . We also included the Lindblad terms for single-spin relaxation and dephasing.

We now have an immediate problem: even with no signal (i.e.  $\phi = 0$ ), the collective loss will cause  $S_z$  to grow in magnitude during the amplification part of the protocol. This will result in a relatively large contribution to  $S_y$  that is indistinguishable from the presence of a signal. An approximate mean-field treatment shows that, for  $\phi \ll 1$  and short times, the average of  $\hat{S}_z$  has the form

$$S_z = \frac{N}{2}\phi - \frac{N(N+1)}{4}\Gamma_{\text{coll}}t. \quad (34)$$

In the limit of interest  $\phi \rightarrow 0$ , the average  $z$  polarization induced by relaxation will completely dominate the contribution from the signal  $\phi$ , which translates into the final measured quantity  $S_y$  being swamped by a large  $\phi$ -independent contribution. This behaviour is indeed seen in full numerical simulations of the dynamics, as depicted in Fig. 9(a). Note that

single-spin relaxation will have an analogous effect here to collective relaxation.

One might think that this problem is merely a technicality, that could be dealt with by simply subtracting off the  $\phi$ -independent background. However, this would require an extremely precise calibration that would be difficult if not impossible to reliably implement in most cases of interest. Alternatively, one could try to reduce the deleterious impact of  $\Gamma_{\text{coll}}$  by using a very large detuning  $\Delta$  (since  $\Gamma_{\text{coll}}/\chi \propto 1/\Delta$ ). This strategy is also not effective if there is any appreciable single-spin dissipation. Consider for example the case where there is non-zero single-spin dephasing at a rate  $\gamma_{\phi}$ . In this case (and neglecting for a moment collective loss, i.e.  $\Gamma = 0$ ), one can show using the exact solution of the master equation (33) reported in Refs. [56, 57] that the gain  $G(t)$  of the OAT protocol is reduced by an exponential factor,

$$G^{\text{OAT}}(t)|_{\gamma_{\phi}>0} = e^{-\gamma_{\phi}t} G^{\text{OAT}}(t)|_{\gamma_{\phi}=0}. \quad (35)$$

To obtain a large gain  $G^{\text{OAT}}(t) \propto \sqrt{N}$ , it is thus crucial that  $t_{\text{OAT}}$  be at most of the order of  $1/\gamma_{\phi}$ , which precludes the use of indefinitely large detuning.

To study the joint impact of both collective and local relaxation in more detail, we use MFT and consider the gain after background subtraction,

$$G_{\text{sub}}^{\text{OAT}}(t) \equiv \lim_{\phi \rightarrow 0} \frac{\delta \langle \hat{S}_y(t) \rangle}{\frac{N\phi}{2}} = \frac{2}{N} \partial_{\phi} \langle \hat{S}_y(t, \phi) \rangle, \quad (36)$$

where  $\delta \langle \hat{S}_y(t) \rangle = \langle \hat{S}_y(t, \phi) \rangle - \langle \hat{S}_y(t, 0) \rangle$  denotes the signal after background subtraction. Figure 9(b) shows  $G_{\text{sub}}^{\text{OAT}}(t)$  (evaluated at its first peak at time  $t = \tau_1$ , see inset of Fig. 9(a)) as a function of the single-spin cooperativity  $\eta_k \equiv \Gamma_{\text{coll}}/\gamma_k$ , where  $k \in \{\phi, \text{rel}\}$ . For each data point, we optimize over the detuning  $\Delta$  and the optimal values are shown in the inset of Fig. 9(b). While the inset of Fig. 9(a) suggests that local maxima of  $G_{\text{sub}}^{\text{OAT}}(t)$  beyond the first peak at  $t = \tau_1$  may lead to larger amplification, this is an artifact of having no single-spin dissipation. By integrating the quantum master equation (33) numerically for  $N = 20$  spins, we have explicitly verified that the performance of the OAT amplification scheme is not improved by considering time evolution past the first maximum of  $G_{\text{sub}}^{\text{OAT}}(t)$  if local dissipation is taken into account (i.e. the first gain peak at  $t = \tau_1$  is the optimal choice). In the presence of both collective and local dissipation, we find that amplification in the OAT scheme is strongly reduced unless the *single-spin* cooperativity satisfies  $\eta_{\phi} \gg \sqrt{N}$  or  $\eta_{\text{rel}} \gg N^{0.9}$  (see Supplemental). Note that this condition becomes harder to saturate if the spin number  $N$  grows. This is in sharp contrast to our dissipative amplification scheme, which

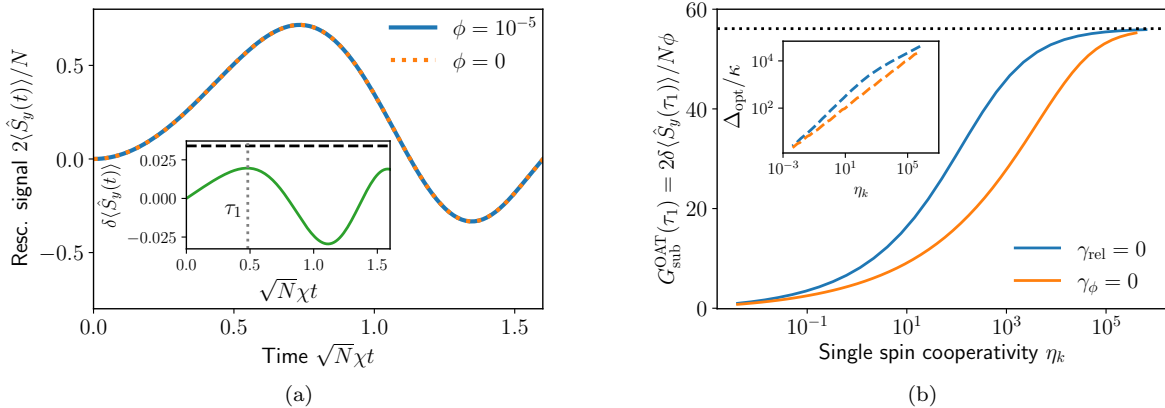


FIG. 9. Analysis of the OAT spin amplification protocol proposed in Ref. [19] for an ensemble of  $N$  standard two-level systems coupled to a detuned bosonic mode via a Tavis-Cummings coupling. The initial signal is encoded in  $\langle \hat{S}_z \rangle$ , whose value is then transduced to  $\langle \hat{S}_y \rangle$  with gain, see Eq. (31). **(a)** Time evolution of  $\langle \hat{S}_y \rangle$ , both with (solid blue curve) and without (dashed orange curve) an initial small signal  $\phi$  (obtained by numerically exact solution of the master equation (33) for  $N = 500$ ,  $\Gamma_{\text{coll}}/\chi = 0.02$ , and  $\gamma_{\text{rel}}/\chi = \gamma_{\phi}/\chi = 0$ ). Collective decay leads to a large average value of  $\langle \hat{S}_y \rangle$  even without any initial signal  $\phi$ . The inset shows the tiny signal obtained after subtraction of this background,  $\delta\langle \hat{S}_y(t) \rangle = \langle \hat{S}_y(t, \phi) \rangle - \langle \hat{S}_y(t, 0) \rangle$ . The black dashed line is the optimal gain one could reach in the absence of collective dissipation. **(b)** Scaling of the gain after background subtraction,  $G_{\text{sub}}^{\text{OAT}}(\tau_1)$ , in the presence of collective decay and either single-spin dephasing (blue curve) or single-spin relaxation (orange curve) as a function of the respective single-spin cooperativity  $\eta_k \equiv \Gamma_{\text{coll}}/\gamma_k$  with  $k \in \{\phi, \text{rel}\}$ . We evaluate the gain at its first peak at time  $t = \tau_1$  (indicated in the inset of (a) by the gray dotted vertical line), which is the time of maximum gain if local dissipation is taken into account. The gain  $G_{\text{sub}}^{\text{OAT}}(\tau_1)$  is strongly reduced compared to its ideal value in the absence of dissipation (dotted black line; note that MFT predicts this quantity to be slightly smaller than master-equation simulations), unless the *single-spin* cooperativity satisfies  $\eta_{\phi} \gg \sqrt{N}$  or  $\eta_{\text{rel}} \gg N^{0.9}$  (see Supplemental). Simulations were done using MFT for  $N = 10^4$  spins. For each  $\eta_k$ , the detuning  $\Delta$  was optimized with the optimized values shown in the inset.

only requires the *collective* cooperativity to satisfy  $C_k \gg 1$ . We thus find that the OAT amplification scheme is of extremely limited utility in the standard case where dissipative two-level systems have a Tavis-Cummings coupling to a common bosonic mode: even if one could perform the subtraction of a large  $\phi$ -independent background, achieving maximum amplification requires an unrealistically large value of the single-spin cooperativity.

We stress that, as already discussed in Ref. [19], one can largely circumvent the above problems by using spin ensembles where each constituent spin has more than two levels. For instance, one can then use two extremely long-lived ground-state spin levels for the sensing and generate the OAT interaction using an auxiliary third level of each spin and a driven cavity [58]. In this case, cavity decay does not lead to a collective relaxation process, only collective dephasing. Since there is no net tendency for  $S_z$  to relax, one does not need to do a large, calibrated background subtraction. Aspects of the effect of the collective dephasing (as well as incoherent spin flips generated by spontaneous emission) were analyzed in Ref. [19]. While this general approach is

well suited to several atomic platforms, it is more restrictive than the case we analyze, where we simply require an ensemble of two-level systems.

## B. Experimental implementations

The focus of this paper is not on one specific experimental platform, but is rather to illuminate the general physics of the collective spin amplification process, a mechanism relevant to many different potential systems. While there are many AMO platforms capable of realizing our resonant, dissipative Tavis-Cummings model, we wish to particularly highlight potential solid-state implementations based on defect spins. These systems have considerable promise in the context of quantum sensing, but usually suffer from the practical obstacle that the ensemble readout is far above the SQL [16].

We start by noting that recent work has experimentally demonstrated superradiance effects in sensing-compatible solid-state spin ensembles [59, 60]. Angerer *et al.* [60] demonstrated superradiant optical emission from  $N \approx 10^{16}$  negatively charged

NV centers, which were homogeneously coupled to a microwave cavity mode in the fast cavity limit, i.e. with a decay rate  $\kappa$  much larger than all other characteristic rates in the system. Instead of a microwave cavity mode, the bosonic mode  $\hat{a}$  could also be implemented by a mechanical mode that is strain-coupled to defect centers [61], e.g. employing mechanical cantilevers [43], optomechanical crystals [45], bulk resonators [44], or surface-acoustic-wave resonators [62]. In addition to NV centers, silicon vacancy (SiV) defect centers could be used [63, 64], which offer larger and field-tunable spin-mechanical coupling rates. Superradiant amplification could then pave a way to dramatically reduce the detrimental impact of detection noise and to approach SQL scaling.

### C. Conclusion

In this work, we have proposed and analyzed a simple yet powerful protocol to reduce the detrimental impact of readout noise in quantum metrology protocols. Unlike previous ideas for spin amplification, our protocol is effective for dissipative ensembles of standard two-level systems, and does not require a large single-spin cooperativity. It allows a system with a highly inefficient spin readout to ultimately reach the SQL within a factor of two.

Our protocol uses the well-known physics of superradiant decay for a new task, namely, amplification of a signal encoded initially in any transverse component of a spin ensemble. In contrast to usual treatments of superradiance, we are not interested in the emitted radiation. Instead, we use superradiance as a tool to induce nonlinear amplification dynamics in the spin system. The gain factor of our protocol achieves the maximum possible scaling,  $G_{\max} \propto \sqrt{N}$  in the large- $N$  limit. The added noise associated the amplification is close to the minimum allowed value one would expect for a quantum-limited bosonic amplifier. While single-spin dissipation and finite temperature do reduce the gain, they do not change the fundamental scaling  $\propto \sqrt{N}$ . In the case of single-spin dissipation, we stress that maximum gain can be achieved by having a large collective cooperativity, i.e. one does *not* need a large single-spin cooperativity. Our protocol is compatible with standard dynamical decoupling techniques to mitigate inhomogeneous broadening effects. Note that another unique aspect of our scheme is that it amplifies all spin directions perpendicular to the  $z$  axis equally (as opposed to only amplifying a single direction in spin space). This could potentially be a useful tool in measurement schemes beyond generalized Ramsey protocols.

Our work also suggests several fruitful directions for future work. For example, combining dissipative spin-amplification techniques with spin squeezing, one could potentially achieve near-Heisenberg-limited sensitivity in systems with highly imperfect spin readout. On a fundamental level, the intrinsic nonlinearity of spin systems requires generalizations of the existing bounds on added noise of phase-preserving amplifiers. The fact the amount of added noise is very similar both in the purely dissipative case and in the coherent  $\kappa \rightarrow 0$  limit may hint at a more fundamental reason to explain the numerically found level of  $\sigma_{\text{add}}^2 \approx 1.3$ . Regarding experimental platforms for quantum sensing, it would also be interesting to study the dynamics and utility of dissipative spin amplification in ensembles where intrinsic dipolar spin-spin interactions are strong.

## IV. MATERIALS AND METHODS

### A. Details on the sensitivity analysis

Here, we provide a detailed derivation of the readout model. We consider a generic situation where the overall measurement result  $n \equiv \sum_{j=1}^N n_j$  is the sum of  $N$  independent measurement results  $n_j$  which are collected in parallel from each spin. Each individual result  $n_j$  depends on the quantum state of the corresponding spin  $j$  in the measurement basis. In the example of fluorescent readout discussed below, this will be the  $z$  basis, i.e.  $\hat{\sigma}_z^{(j)}|\sigma_j\rangle = \sigma_j|\sigma_j\rangle$  with  $\sigma_j = \pm 1$ . However, we will keep the measurement basis general for now.

We assume that the probability distribution of the measurement result  $n_j$  depends on the state of spin  $j$ . Specifically, if spin  $j$  is in an eigenstate  $|\sigma_j\rangle$  of the measurement basis, the corresponding measurement result  $n_j$  will be distributed according to the state-dependent probability distribution  $\mathcal{P}_{\sigma_j}(n_j)$ . For a general pure single-spin state  $|\psi_j\rangle = \sum_{\sigma_j} c_{\sigma_j}|\sigma_j\rangle$ , we assume that the  $n_j$  will be distributed according to the weighted sum of these probability distributions,  $\mathcal{P}_{|\psi_j\rangle}(n_j) = \sum_{\sigma_j} |c_{\sigma_j}|^2 \mathcal{P}_{\sigma_j}(n_j)$ . The probability distributions  $\mathcal{P}_{\sigma_j}(n_j)$  depend on the specific measurement protocol and we will leave them general for now, too. Note that this approach is equivalent to a POVM with a separate measurement operator  $\hat{M}_{n_j, \sigma_j} = \sqrt{\mathcal{P}_{\sigma_j}(n_j)}|\sigma_j\rangle\langle\sigma_j|$  for each value of  $\sigma_j$ . The effect corresponding to the observation of  $n_j$  photons is then given by  $\hat{E}_{n_j} = \sum_{\sigma_j} \mathcal{P}_{\sigma_j}(n_j)|\sigma_j\rangle\langle\sigma_j|$ . However, since the addition of readout noise is a classical process, a POVM is not necessarily needed to model it.

Given an ensemble of  $N$  spins, the probabil-

ity distribution of the overall measurement result  $n = \sum_{j=1}^N n_j$  for a product state  $|\sigma_1, \dots, \sigma_N\rangle$  in the measurement basis is the convolution of all single-spin probability distributions,  $\mathcal{P}_{\sigma_1, \dots, \sigma_N}(n) = (*_{j=1}^N \mathcal{P}_{\sigma_j})(n)$ . Similar to the single-spin case, we assume that the probability distribution of  $n$  for a general pure  $N$ -spin state

$$|\psi\rangle = \sum_{\{\sigma_j\}} c_{\sigma_1, \dots, \sigma_N} |\sigma_1, \dots, \sigma_N\rangle \quad (37)$$

is given by the average

$$\mathcal{P}_{|\psi\rangle}(n) = \sum_{\{\sigma_j\}} |c_{\sigma_1, \dots, \sigma_N}|^2 \mathcal{P}_{\sigma_1, \dots, \sigma_N}(n). \quad (38)$$

The corresponding POVM has the measurement operators  $\hat{M}_{\{n_j\}, \{\sigma_j\}} = \otimes_{j=1}^N \sqrt{\mathcal{P}_{\sigma_j}(n_j)} |\sigma_j\rangle \langle \sigma_j|$  for each possible combination  $\{\sigma_j\}$ . Since we are only observing the total photon number  $n = \sum_{j=1}^N n_j$ , the effects are  $\hat{E}_n = \sum'_{\{n_j\}} \sum_{\{\sigma_j\}} \hat{M}_{\{n_j\}, \{\sigma_j\}}^\dagger \hat{M}_{\{n_j\}, \{\sigma_j\}}$  where  $\sum'_{\{n_j\}}$  denotes a sum over all possible combinations of  $\{n_j\}$  such that  $\sum_{j=1}^N n_j = n$ .

We are now interested in the fluctuations of  $n$  with respect to the probability distribution (38),

$$\begin{aligned} (\Delta n)^2 &\equiv \sum_n n^2 \mathcal{P}_{|\psi\rangle}(n) - \left( \sum_n n \mathcal{P}_{|\psi\rangle}(n) \right)^2 \\ &= \sum_n \sum_{\{\sigma_j\}} n^2 |c_{\sigma_1, \dots, \sigma_N}|^2 \mathcal{P}_{\sigma_1, \dots, \sigma_N}(n) \\ &\quad - \left( \sum_n \sum_{\{\sigma_j\}} n |c_{\sigma_1, \dots, \sigma_N}|^2 \mathcal{P}_{\sigma_1, \dots, \sigma_N}(n) \right)^2. \end{aligned} \quad (39)$$

The second line shows that calculating a moment  $n^m$  of the probability distribution (38) involves two different averages: First, a  $n$ -average with respect to the classical conditional probability distribution  $\mathcal{P}_{\sigma_1, \dots, \sigma_N}(n)$  describing the readout for a particular spin configuration  $\{\sigma_j\}$  in the measurement basis. We will denote this average by

$$\mathbf{E}_{\{\sigma_j\}}[n^m] \equiv \sum_n n^m \mathcal{P}_{\sigma_1, \dots, \sigma_N}(n). \quad (40)$$

Second, an average of the classical expectation values  $\mathbf{E}_{\{\sigma_j\}}[n^m]$  with respect to the probabilities  $|c_{\sigma_1, \dots, \sigma_N}|^2$  to obtain a certain spin configuration  $\{\sigma_j\}$  in the quantum state (37). This is the step where the properties of the quantum state  $|\psi\rangle$  enter and we will denote this average by

$$\langle f_{\{\sigma_j\}} \rangle_{|\psi\rangle} \equiv \sum_{\{\sigma_j\}} |c_{\sigma_1, \dots, \sigma_N}|^2 f_{\{\sigma_j\}}, \quad (41)$$

where  $f_{\{\sigma_j\}}$  is a function that depends on the spin configuration  $\{\sigma_j\}$ . Note that this does not look like the typical quantum expectation value of an observable with respect to the quantum state  $|\psi\rangle$ . However, for a specific readout model, the moments of the probability distribution  $\mathcal{P}_{\sigma_1, \dots, \sigma_N}(n)$  will be related to moments of an observable of the quantum state: for instance, in the case of fluorescent readout discussed below, this will be the spin component  $\hat{S}_z$ . Therefore, the expectation value  $\langle f_{\{\sigma_j\}} \rangle_{|\psi\rangle}$  will turn into a familiar quantum expectation value. With these definitions at hand, the variance of  $n$  given by Eq. (39) can be rewritten as follows:

$$\begin{aligned} (\Delta n)^2 &= \langle \mathbf{E}_{\{\sigma_j\}}[n^2] \rangle_{|\psi\rangle} - \langle \mathbf{E}_{\{\sigma_j\}}[n] \rangle_{|\psi\rangle}^2 \\ &= \left( \langle \mathbf{E}_{\{\sigma_j\}}[n^2] \rangle_{|\psi\rangle} - \langle \mathbf{E}_{\{\sigma_j\}}[n]^2 \rangle_{|\psi\rangle} \right) \\ &\quad + \left( \langle \mathbf{E}_{\{\sigma_j\}}[n^2] \rangle_{|\psi\rangle} - \langle \mathbf{E}_{\{\sigma_j\}}[n] \rangle_{|\psi\rangle}^2 \right), \end{aligned} \quad (42)$$

where we added a zero in the last line. The first term in Eq. (42) describes the classical noise which is added by the detector due to the fact that  $\mathcal{P}_{\sigma_1, \dots, \sigma_N}(n)$  has a finite variance for each basis state  $|\sigma_1, \dots, \sigma_N\rangle$ . The second term represents the variance of  $\mathbf{E}_{\{\sigma_j\}}[n]$  due to the intrinsic fluctuations of the state  $|\psi\rangle$ , i.e. its intrinsic spin-projection noise expressed in terms of the measured quantity  $n$ .

Likewise, the average measurement result can be expressed as follows:

$$\bar{n} \equiv \sum_n n \mathcal{P}_{|\psi\rangle}(n) = \langle \mathbf{E}_{\{\sigma_j\}}[n] \rangle_{|\psi\rangle}. \quad (43)$$

The change of  $\bar{n}$  with respect to the signal  $\phi$ ,  $\partial_\phi \bar{n}$ , is the transduction factor that we need to refer the measurement error  $(\Delta n)^2$  back to the signal:

$$\begin{aligned} (\Delta \phi)^2 &= \frac{(\Delta n)^2}{|\partial_\phi \bar{n}|^2} \\ &= \frac{\langle \mathbf{E}_{\{\sigma_j\}}[n^2] \rangle_{|\psi\rangle} - \langle \mathbf{E}_{\{\sigma_j\}}[n] \rangle_{|\psi\rangle}^2}{|\partial_\phi \langle \mathbf{E}_{\{\sigma_j\}}[n] \rangle_{|\psi\rangle}|^2} \\ &\quad + \frac{\langle \mathbf{E}_{\{\sigma_j\}}[n^2] \rangle_{|\psi\rangle} - \langle \mathbf{E}_{\{\sigma_j\}}[n] \rangle_{|\psi\rangle}^2}{|\partial_\phi \langle \mathbf{E}_{\{\sigma_j\}}[n] \rangle_{|\psi\rangle}|^2}. \end{aligned} \quad (44)$$

Note that both the numerator and denominator in the second term are expressed using only  $\mathbf{E}_{\{\sigma_j\}}[n]$ , i.e. if  $n$  is related to some spin observable  $\hat{O}$  by a linear transformation, the conversion factors will drop out and the second term will become the bare spin-projection noise with respect to  $\hat{O}$ .

For concreteness, we specialize this result to the case of fluorescent readout [16]. In this case, the quantity  $n$  denotes the number of detected photons and  $\mathcal{P}_{|\sigma_j\rangle}(n_j)$  is a Poissonian distribution with mean  $n_b$  ( $n_d$ ) if spin  $j$  is in the bright (dark) state. The



overall measurement result  $n$  also follows a Poissonian distribution with expectation value

$$\mathbf{E}_{\{\sigma_j\}}[n] = N_b n_b + N_d n_d, \quad (45)$$

where  $N_b$  ( $N_d$ ) denotes the number of spins in the bright (dark) state. Using the basis  $|j, m\rangle$  of simultaneous eigenstates of  $\hat{\mathbf{S}}^2$  and  $\hat{S}_z$ , one can rewrite the state (37) as  $|\psi\rangle = \sum_j \sum_{m=-j}^j c_m^j |j, m\rangle$ . Assuming the ground state of each spin is the bright state, we then have  $N_b = N/2 - m$  and  $N_d = N/2 + m$  and obtain

$$\langle \mathbf{E}_{\{\sigma_j\}}[n] \rangle_{|\psi\rangle} = N n_{\text{avg}} \left[ 1 + \frac{2}{N} \langle \hat{S}_z \rangle \tilde{C} \right], \quad (46)$$

where  $n_{\text{avg}} = (n_b + n_d)/2$  is the average number of emitted photons and  $\tilde{C} = (n_b - n_d)/(n_b + n_d)$  is the contrast between the bright and the dark state [8, 16, 65]. Evaluating Eq. (44), we find

$$(\Delta\phi)^2 = \frac{\frac{N}{4} \frac{1+2\tilde{C}\langle\hat{S}_z\rangle/N}{\tilde{C}^2 n_{\text{avg}}}}{|\partial_\phi \langle \hat{S}_z \rangle|^2} + \frac{\langle \hat{S}_z^2 \rangle - \langle \hat{S}_z \rangle^2}{|\partial_\phi \langle \hat{S}_z \rangle|^2}. \quad (47)$$

For a small signal  $\langle \hat{S}_z \rangle = N\phi/2$  with  $\phi \ll 1$ , one can ignore the second term in the numerator of the detection noise contribution. Note that these equations are given in terms of the basis of the final measurement at times  $t_3 < t \leq t_4$  in Fig. 1(a), which is the  $\hat{S}_z$  spin component. In the main text, we discuss everything in terms of the final state of the amplification step at  $t = t_3$ . It differs from the measured state by the  $\pi/2$  rotation at  $t = t_3$ , which maps  $\hat{S}_y \rightarrow \hat{S}_z$  and  $(\Delta S_y)^2 \rightarrow (\Delta S_z)^2$ .

To discuss the scaling of the two terms in Eq. (47), we focus on two typical probe states in a Ramsey experiment: CSS and spin-squeezed states.

For a CSS, the slope of the signal depends on the length of the spin vector,  $|\partial_\phi \langle \hat{S}_z \rangle| = N/2$ , i.e. the first (detection noise) term has an SQL-like scaling  $1/\tilde{C}^2 n_{\text{avg}} N \propto 1/N$  with a readout-dependent prefactor  $1/\tilde{C}^2 n_{\text{avg}}$ . The CSS variance is  $(\Delta S_z)^2 = N/4$ , therefore, the second (projection-noise) term reduces to  $1/N$ . In the absence of amplification, the measurement error  $(\Delta\phi)^2$  thus has a SQL-like  $1/N$  scaling with a readout-noise-dependent prefactor  $1 + 1/\tilde{C}^2 n_{\text{avg}}$ .

For a spin-squeezed state, the slope of the signal depends on the effective length of the spin vector along the mean spin direction  $|\partial_\phi \langle \hat{S}_z \rangle| = |\langle \hat{S}_{\text{msd}} \rangle| \leq N/2$ . Since a spin-squeezed state wraps around the Bloch sphere for sufficiently large squeezing,  $|\langle \hat{S}_{\text{msd}} \rangle|$  decreases with increasing squeezing strength. The first (detection-noise) term thus reduces to

$$\frac{1}{\tilde{C}^2 n_{\text{avg}} N} \left( \frac{N/2}{|\langle \hat{S}_{\text{msd}} \rangle|} \right)^2, \quad (48)$$

i.e. detection noise is *larger* for a spin-squeezed state than for a simple CSS if squeezing is sufficiently strong to reduce  $|\langle \hat{S}_{\text{msd}} \rangle|$ . The second (projection-noise) term can be expressed as  $\xi_R^2/N$ , where we introduced the Wineland parameter  $\xi_R^2 = N \min_{\perp} (\Delta S_{\perp})^2 / |\langle \hat{S}_{\text{msd}} \rangle|^2$  and  $\perp$  denotes the directions perpendicular to the mean-spin direction [13, 14, 66]. Using spin squeezing, one can push the Wineland parameter below unity such that the projection noise reaches at best a Heisenberg-like  $1/N^2$  scaling. Note that, in the presence of a very bad readout  $1/\tilde{C}^2 n_{\text{avg}} \gg 1$ , this optimizes an almost irrelevant term of the overall measurement error and thus does not improve  $(\Delta\phi)^2$  significantly. As a consequence, the overall measurement error  $(\Delta\phi)^2$  still scales  $\propto 1/N$  and the loss of signal slope,  $|\langle \hat{S}_{\text{msd}} \rangle| \rightarrow 0$ , increases the detrimental impact of detection noise beyond the level one would have observed for a simple CSS probe state. Hence, spin squeezing is not a useful strategy if readout noise dominates.

Finally, we give typical values for the readout-noise prefactor  $1/\tilde{C}^2 n_{\text{avg}}$ . For fluorescent readout in trapped-ion setups [47], the decay of the dark state into the bright state is slow enough to allow for sufficiently long integration times such that  $n_{\text{avg}} \approx 30$  and  $\tilde{C} \approx 98\%$  [67], yielding a strong suppression of detection noise by a factor of  $1/\tilde{C}^2 n_{\text{avg}} \approx 0.03 \ll 1$ . However, the situation is dramatically different for solid-state defects, e.g. negatively charged NV defects in diamond [16]. Here, fluorescent readout leads to a rapid polarization of the NV spin into the bright state, such that the best values even for a *single* NV center are  $n_{\text{avg}} \approx 0.3$  and  $\tilde{C} \approx 15\%$  [16, 65]. Therefore, the detection noise dominates the over projection noise by a factor of  $1/\tilde{C}^2 n_{\text{avg}} \approx 150$ . For ensembles of many NV centers, the detrimental impact of readout noise is even larger: the best reported value is  $1/\tilde{C}^2 n_{\text{avg}} \approx 67^2 \approx 4500$  [16, 68].

## B. Mean-field theory analysis

To gain intuition on the amplification dynamics, we use MFT to derive approximate nonlinear equations of motion for the system. The differential equations for the spin components  $S_k = \langle \hat{S}_k \rangle$ , where  $k \in \{x, y, z\}$ , generate an (infinite) hierarchy of coupled differential equations for higher-order spin correlation functions, which we truncate and close by performing a second-order cumulant expansion [69]. This treatment is exact if the state is Gaussian.

We start with the quantum master equation

$$\begin{aligned} \frac{d\hat{\rho}}{dt} = & \Gamma(n_{\text{th}} + 1)\mathcal{D}[\hat{S}_-]\hat{\rho} + \Gamma n_{\text{th}}\mathcal{D}[\hat{S}_+]\hat{\rho} \\ & + \gamma_{\text{rel}} \sum_{i=1}^N \mathcal{D}[\hat{\sigma}_-^{(i)}]\hat{\rho} + \frac{\gamma_{\phi}}{2} \sum_{j=1}^N \mathcal{D}[\hat{\sigma}_z^{(j)}]\hat{\rho}. \end{aligned} \quad (49)$$

Without loss of generality, we take the initial state to be  $e^{i\phi\hat{S}_x}|\uparrow \dots \uparrow\rangle$ . This initial state has  $S_x(t) = C_{xy}(t) = C_{xz}(t) = 0$ , where the covariances are defined by  $C_{kl} \equiv \langle(\hat{S}_k\hat{S}_l + \hat{S}_l\hat{S}_k)\rangle/2 - \langle\hat{S}_k\rangle\langle\hat{S}_l\rangle$  for  $k, l \in \{x, y, z\}$ . Since we are interested in the limit of a very small signal,  $\phi \ll 1$ , we drop all terms of the order  $\phi^2$  in the initial conditions and in the equations of motion, which implies  $C_{xx}(t) = C_{yy}(t)$ . The mean-field equations are then given by

$$\dot{S}_y = -\left[\frac{\Gamma}{2} + \Gamma n_{\text{th}} - \Gamma S_z + \gamma_{\phi} + \frac{\gamma_{\text{rel}}}{2}\right] S_y + \Gamma C_{yz}, \quad (50)$$

$$\dot{S}_z = -\Gamma(1 + 2n_{\text{th}})S_z - 2\Gamma C_{xx} - \gamma_{\text{rel}}\left(S_z + \frac{N}{2}\right), \quad (51)$$

$$\begin{aligned} \dot{C}_{xx} = & -[\Gamma(1 + 2n_{\text{th}}) + 2\gamma_{\phi} + \gamma_{\text{rel}} - 2\Gamma S_z] C_{xx} \\ & + \Gamma(1 + 2n_{\text{th}})S_z^2 - \frac{\Gamma}{2}S_z + \frac{N}{2}\left(\gamma_{\phi} + \frac{\gamma_{\text{rel}}}{2}\right), \end{aligned} \quad (52)$$

$$\dot{C}_{zz} = +2\Gamma(1 + 2n_{\text{th}})C_{xx} + (\Gamma + \gamma_{\text{rel}})S_z + \frac{\gamma_{\text{rel}}}{2}N, \quad (53)$$

$$\begin{aligned} \dot{C}_{yz} = & -\left[\frac{5}{2}\Gamma(1 + 2n_{\text{th}}) - \Gamma S_z + \gamma_{\phi} + \frac{3}{2}\gamma_{\text{rel}}\right] C_{yz} \\ & - \left[\Gamma(1 + 2n_{\text{th}})S_z + 2\Gamma C_{xx} - \frac{\Gamma}{4} - \frac{\gamma_{\text{rel}}}{2}\right] S_y. \end{aligned} \quad (54)$$

For simplicity, we ignore local dissipation for now,  $\gamma_{\text{rel}} = \gamma_{\phi} = 0$ . Then, the equations of motion con-

serve total angular momentum,

$$\frac{N}{2}\left(\frac{N}{2} + 1\right) = 2C_{xx} + S_z^2 + C_{zz}, \quad (55)$$

where  $C_{zz}$  is found to be suppressed by an order of  $N$  compared to  $C_{xx}$  and  $S_z^2$ . We thus drop  $C_{zz}$  and use Eq. (55) to eliminate the covariance  $C_{xx}$  from the mean-field equations. This step decouples the equation of motion for  $S_z$  from the rest of the system, but the equation of motion of  $S_y$  still depends on the covariance  $C_{yz}$ . At short times,  $C_{yz}$  is suppressed compared to the  $S_z S_y$  term by a factor of  $N$ , therefore, we drop it from the equation of motion. In this way, we obtain a very simple set of equations of motion for  $S_y$  and  $S_z$ :

$$\dot{S}_y = -\Gamma\left[\frac{1}{2} + n_{\text{th}} - S_z\right] S_y, \quad (56)$$

$$\dot{S}_z = -\Gamma\left[\frac{N}{2}\left(\frac{N}{2} + 1\right) + S_z(1 + 2n_{\text{th}} - S_z)\right]. \quad (57)$$

The solutions predict the exact dynamics (determined by numerically exact solution of the quantum master equation (49)) qualitatively correct, i.e. they allow us to derive the scaling laws in  $N$  up to numerical prefactors. Note that Eq. (57) for  $n_{\text{th}} = 0$  has already been obtained in the literature on superradiance using other derivations [36, 37].

## ACKNOWLEDGMENTS

We acknowledge discussions with A. Bleszynski Jayich, J. V. Cady, C. Padgett, V. Dharod, H. Oh, and Y. Tsaturyan. This work was supported by the DARPA DRINQS program (Agreement D18AC00014).

- 
- [1] M. H. Schleier-Smith, I. D. Leroux, and V. Vuletić, States of an ensemble of two-level atoms with reduced quantum uncertainty, *Phys. Rev. Lett.* **104**, 073604 (2010).  
 [2] K. C. Cox, G. P. Greve, J. M. Weiner, and J. K. Thompson, Deterministic squeezed states with collective measurements and feedback, *Phys. Rev. Lett.* **116**, 093602 (2016).  
 [3] O. Hosten, R. Krishnakumar, N. J. Engelsen, and M. A. Kasevich, Quantum phase magnification, *Science* **352**, 1552 (2016).  
 [4] V. M. Acosta, E. Bauch, M. P. Ledbetter, C. Santori, K.-M. C. Fu, P. E. Barclay, R. G. Beausoleil,

- H. Linget, J. F. Roch, F. Treussart, S. Chemerisov, W. Gawlik, and D. Budker, Diamonds with a high density of nitrogen-vacancy centers for magnetometry applications, *Phys. Rev. B* **80**, 115202 (2009).  
 [5] S. Steinert, F. Dolde, P. Neumann, A. Aird, B. Naydenov, G. Balasubramanian, F. Jelezko, and J. Wrachtrup, High sensitivity magnetic imaging using an array of spins in diamond, *Review of Scientific Instruments* **81**, 043705 (2010).  
 [6] L. M. Pham, D. L. Sage, P. L. Stanwix, T. K. Yeung, D. Glenn, A. Trifonov, P. Cappellaro, P. R. Hemmer, M. D. Lukin, H. Park, A. Yacoby, and R. L. Walsworth, Magnetic field imaging with nitrogen-

- vacancy ensembles, *New Journal of Physics* **13**, 045021 (2011).
- [7] T. Wolf, P. Neumann, K. Nakamura, H. Sumiya, T. Ohshima, J. Isoya, and J. Wrachtrup, Subpicotesla diamond magnetometry, *Phys. Rev. X* **5**, 041001 (2015).
- [8] J. M. Taylor, P. Cappellaro, L. Childress, L. Jiang, D. Budker, P. R. Hemmer, A. Yacoby, R. Walsworth, and M. D. Lukin, High-sensitivity diamond magnetometer with nanoscale resolution, *Nature Physics* **4**, 810 (2008).
- [9] L. Rondin, J.-P. Tetienne, T. Hingant, J.-F. Roch, P. Maletinsky, and V. Jacques, Magnetometry with nitrogen-vacancy defects in diamond, *Reports on Progress in Physics* **77**, 056503 (2014).
- [10] F. Dolde, H. Fedder, M. W. Doherty, T. Nöbauer, F. Rempp, G. Balasubramanian, T. Wolf, F. Reinhard, L. C. L. Hollenberg, F. Jelezko, and J. Wrachtrup, Electric-field sensing using single diamond spins, *Nature Physics* **7**, 459 (2011).
- [11] V. M. Acosta, E. Bauch, M. P. Ledbetter, A. Waxman, L.-S. Bouchard, and D. Budker, Temperature dependence of the nitrogen-vacancy magnetic resonance in diamond, *Phys. Rev. Lett.* **104**, 070801 (2010).
- [12] M. Kitagawa and M. Ueda, Squeezed spin states, *Phys. Rev. A* **47**, 5138 (1993).
- [13] J. Ma, X. Wang, C. Sun, and F. Nori, Quantum spin squeezing, *Physics Reports* **509**, 89 (2011).
- [14] L. Pezzè, A. Smerzi, M. K. Oberthaler, R. Schmied, and P. Treutlein, Quantum metrology with nonclassical states of atomic ensembles, *Rev. Mod. Phys.* **90**, 035005 (2018).
- [15] C. L. Degen, F. Reinhard, and P. Cappellaro, Quantum sensing, *Rev. Mod. Phys.* **89**, 035002 (2017).
- [16] J. F. Barry, J. M. Schloss, E. Bauch, M. J. Turner, C. A. Hart, L. M. Pham, and R. L. Walsworth, Sensitivity optimization for nv-diamond magnetometry, *Rev. Mod. Phys.* **92**, 015004 (2020).
- [17] C. M. Caves, Quantum limits on noise in linear amplifiers, *Phys. Rev. D* **26**, 1817 (1982).
- [18] B. Yurke, S. L. McCall, and J. R. Klauder,  $Su(2)$  and  $su(1,1)$  interferometers, *Phys. Rev. A* **33**, 4033 (1986).
- [19] E. Davis, G. Bentsen, and M. Schleier-Smith, Approaching the heisenberg limit without single-particle detection, *Phys. Rev. Lett.* **116**, 053601 (2016).
- [20] F. Fröwis, P. Sekatski, and W. Dür, Detecting large quantum fisher information with finite measurement precision, *Phys. Rev. Lett.* **116**, 090801 (2016).
- [21] T. Macrì, A. Smerzi, and L. Pezzè, Loschmidt echo for quantum metrology, *Phys. Rev. A* **94**, 010102 (2016).
- [22] E. Davis, G. Bentsen, T. Li, and M. Schleier-Smith, Advantages of interaction-based readout for quantum sensing, in *Advances in Photonics of Quantum Computing, Memory, and Communication X*, Vol. 10118, edited by Z. U. Hasan, P. R. Hemmer, H. Lee, and A. L. Migdall, International Society for Optics and Photonics (SPIE, 2017) pp. 104 – 113.
- [23] S. A. Haine, Using interaction-based readouts to approach the ultimate limit of detection-noise robustness for quantum-enhanced metrology in collective spin systems, *Phys. Rev. A* **98**, 030303 (2018).
- [24] F. Anders, L. Pezzè, A. Smerzi, and C. Klempt, Phase magnification by two-axis counter-twisting for detection-noise robust interferometry, *Phys. Rev. A* **97**, 043813 (2018).
- [25] M. Schulte, V. J. Martínez-Lahuerta, M. S. Scharnagl, and K. Hammerer, Ramsey interferometry with generalized one-axis twisting echoes, *Quantum* **4**, 268 (2020).
- [26] D. Leibfried, M. D. Barrett, T. Schaetz, J. Britton, J. Chiaverini, W. M. Itano, J. D. Jost, C. Langer, and D. J. Wineland, Toward heisenberg-limited spectroscopy with multiparticle entangled states, *Science* **304**, 1476 (2004).
- [27] D. Leibfried, E. Knill, S. Seidelin, J. Britton, R. B. Blakestad, J. Chiaverini, D. B. Hume, W. M. Itano, J. D. Jost, C. Langer, R. Ozeri, R. Reichle, and D. J. Wineland, Creation of a six-atom schrödinger cat state, *Nature* **438**, 639 (2005).
- [28] S. P. Nolan, S. S. Szigeti, and S. A. Haine, Optimal and robust quantum metrology using interaction-based readouts, *Phys. Rev. Lett.* **119**, 193601 (2017).
- [29] D. Linnemann, H. Strobel, W. Muessel, J. Schulz, R. J. Lewis-Swan, K. V. Kheruntsyan, and M. K. Oberthaler, Quantum-enhanced sensing based on time reversal of nonlinear dynamics, *Phys. Rev. Lett.* **117**, 013001 (2016).
- [30] S. C. Burd, R. Srinivas, J. J. Bollinger, A. C. Wilson, D. J. Wineland, D. Leibfried, D. H. Slichter, and D. T. C. Allcock, Quantum amplification of mechanical oscillator motion, *Science* **364**, 1163 (2019).
- [31] A. A. Clerk, M. H. Devoret, S. M. Girvin, F. Marquardt, and R. J. Schoelkopf, Introduction to quantum noise, measurement, and amplification, *Rev. Mod. Phys.* **82**, 1155 (2010).
- [32] R. H. Dicke, Coherence in spontaneous radiation processes, *Phys. Rev.* **93**, 99 (1954).
- [33] A. V. Andreev, V. I. Emel'yanov, and Y. A. Il'inskii, Collective spontaneous emission (dicke superradiance), *Soviet Physics Uspekhi* **23**, 493 (1980).
- [34] M. Gross and S. Haroche, Superradiance: An essay on the theory of collective spontaneous emission, *Physics Reports* **93**, 301 (1982).
- [35] M. G. Benedict, A. M. Ermolaev, V. A. Malyshev, I. V. Sokolov, and E. D. Trifonov, *Super-radiance: multiatomic coherent emission* (CRC Press LLC, 2018).
- [36] G. S. Agarwal, Master-equation approach to spontaneous emission, *Phys. Rev. A* **2**, 2038 (1970).
- [37] N. E. Rehler and J. H. Eberly, Superradiance, *Phys. Rev. A* **3**, 1735 (1971).
- [38] J. G. Bohnet, Z. Chen, J. M. Weiner, D. Meiser, M. J. Holland, and J. K. Thompson, A steady-state superradiant laser with less than one intracavity photon, *Nature* **484**, 78 (2012).
- [39] J. G. Bohnet, Z. Chen, J. M. Weiner, K. C. Cox, and J. K. Thompson, Active and passive sensing of

- collective atomic coherence in a superradiant laser, *Phys. Rev. A* **88**, 013826 (2013).
- [40] J. Riedrich-Möller, L. Kipfstuhl, C. Hepp, E. Neu, C. Pauly, F. Mücklich, A. Baur, M. Wandt, S. Wolff, M. Fischer, S. Gsell, M. Schreck, and C. Becher, One- and two-dimensional photonic crystal microcavities in single crystal diamond, *Nature Nanotechnology* **7**, 69 (2012).
- [41] A. Faraon, C. Santori, Z. Huang, V. M. Acosta, and R. G. Beausoleil, Coupling of nitrogen-vacancy centers to photonic crystal cavities in monocrystalline diamond, *Phys. Rev. Lett.* **109**, 033604 (2012).
- [42] J. C. Lee, I. Aharonovich, A. P. Magyar, F. Rol, and E. L. Hu, Coupling of silicon-vacancy centers to a single crystal diamond cavity, *Opt. Express* **20**, 8891 (2012).
- [43] S. Meesala, Y.-I. Sohn, H. A. Atikian, S. Kim, M. J. Burek, J. T. Choy, and M. Lončar, Enhanced strain coupling of nitrogen-vacancy spins to nanoscale diamond cantilevers, *Phys. Rev. Applied* **5**, 034010 (2016).
- [44] E. R. MacQuarrie, T. A. Gosavi, A. M. Moehle, N. R. Jungwirth, S. A. Bhave, and G. D. Fuchs, Coherent control of a nitrogen-vacancy center spin ensemble with a diamond mechanical resonator, *Optica* **2**, 233 (2015).
- [45] J. V. Cady, O. Michel, K. W. Lee, R. N. Patel, C. J. Sarabalis, A. H. Safavi-Naeini, and A. C. B. Jayich, Diamond optomechanical crystals with embedded nitrogen-vacancy centers, *Quantum Science and Technology* **4**, 024009 (2019).
- [46] G. S. Agarwal, Master-equation approach to spontaneous emission. iii. many-body aspects of emission from two-level atoms and the effect of inhomogeneous broadening, *Phys. Rev. A* **4**, 1791 (1971).
- [47] H. Häffner, C. Roos, and R. Blatt, Quantum computing with trapped ions, *Physics Reports* **469**, 155 (2008).
- [48] H. A. Haus and J. A. Mullen, Quantum noise in linear amplifiers, *Phys. Rev.* **128**, 2407 (1962).
- [49] D. Meiser, J. Ye, D. R. Carlson, and M. J. Holland, Prospects for a millihertz-linewidth laser, *Phys. Rev. Lett.* **102**, 163601 (2009).
- [50] P. Groszkowski, M. Koppenhöfer, H.-K. Lau, and A. A. Clerk, Reservoir-engineered spin squeezing: macroscopic even-odd effects and hybrid-systems implementations, *arXiv* , 2104.10363 (2021), 2104.10363v1.
- [51] A. V. Andreev, V. Gurarie, and L. Radzihovsky, Nonequilibrium dynamics and thermodynamics of a degenerate fermi gas across a feshbach resonance, *Phys. Rev. Lett.* **93**, 130402 (2004).
- [52] R. A. Barankov and L. S. Levitov, Atom-molecule coexistence and collective dynamics near a feshbach resonance of cold fermions, *Phys. Rev. Lett.* **93**, 130403 (2004).
- [53] J. Keeling, Quantum corrections to the semiclassical collective dynamics in the tavis-cummings model, *Phys. Rev. A* **79**, 053825 (2009).
- [54] A. Szorkovszky, A. A. Clerk, A. C. Doherty, and W. P. Bowen, Detuned mechanical parametric amplification as a quantum non-demolition measurement, *New Journal of Physics* **16**, 043023 (2014).
- [55] A. Metelmann and A. A. Clerk, Nonreciprocal photon transmission and amplification via reservoir engineering, *Phys. Rev. X* **5**, 021025 (2015).
- [56] M. Foss-Feig, K. R. A. Hazzard, J. J. Bollinger, and A. M. Rey, Nonequilibrium dynamics of arbitrary-range ising models with decoherence: An exact analytic solution, *Phys. Rev. A* **87**, 042101 (2013).
- [57] A. McDonald and A. A. Clerk, Exact solutions of interacting dissipative systems via weak symmetries, *arXiv preprint* , 2109.13221 (2021).
- [58] I. D. Leroux, M. H. Schleier-Smith, and V. Vuletić, Implementation of cavity squeezing of a collective atomic spin, *Phys. Rev. Lett.* **104**, 073602 (2010).
- [59] C. Bradac, M. T. Johansson, M. v. Breugel, B. Q. Baragiola, R. Martin, M. L. Juan, G. K. Brennen, and T. Volz, Room-temperature spontaneous super-radiance from single diamond nanocrystals, *Nature Communications* **8**, 1205 (2017).
- [60] A. Angerer, K. Streltsov, T. Astner, S. Putz, H. Sumiya, S. Onoda, J. Isoya, W. J. Munro, K. Nemoto, J. Schmiedmayer, and J. Majer, Super-radiant emission from colour centres in diamond, *Nature Physics* **14**, 1168 (2018).
- [61] D. Lee, K. W. Lee, J. V. Cady, P. Ouartchaiyapong, and A. C. B. Jayich, Topical review: spins and mechanics in diamond, *Journal of Optics* **19**, 033001 (2017).
- [62] D. A. Golter, T. Oo, M. Amezcua, I. Lekavicius, K. A. Stewart, and H. Wang, Coupling a surface acoustic wave to an electron spin in diamond via a dark state, *Phys. Rev. X* **6**, 041060 (2016).
- [63] S. Meesala, Y.-I. Sohn, B. Pingault, L. Shao, H. A. Atikian, J. Holzgrafe, M. Gündoğan, C. Stavarakas, A. Sipahigil, C. Chia, R. Evans, M. J. Burek, M. Zhang, L. Wu, J. L. Pacheco, J. Abraham, E. Bielejec, M. D. Lukin, M. Atatüre, and M. Lončar, Strain engineering of the silicon-vacancy center in diamond, *Phys. Rev. B* **97**, 205444 (2018).
- [64] S. Maity, L. Shao, S. Bogdanović, S. Meesala, Y.-I. Sohn, N. Sinclair, B. Pingault, M. Chalupnik, C. Chia, L. Zheng, K. Lai, and M. Loncar, Coherent acoustic control of a single silicon vacancy spin in diamond, *Nature Communications* **11**, 193 (2020).
- [65] B. J. Shields, Q. P. Unterreithmeier, N. P. de Leon, H. Park, and M. D. Lukin, Efficient readout of a single spin state in diamond via spin-to-charge conversion, *Phys. Rev. Lett.* **114**, 136402 (2015).
- [66] D. J. Wineland, J. J. Bollinger, W. M. Itano, F. L. Moore, and D. J. Heinzen, Spin squeezing and reduced quantum noise in spectroscopy, *Phys. Rev. A* **46**, R6797 (1992).
- [67] A. H. Myerson, D. J. Szwer, S. C. Webster, D. T. C. Allcock, M. J. Curtis, G. Imreh, J. A. Sherman, D. N. Stacey, A. M. Steane, and D. M. Lucas, High-fidelity readout of trapped-ion qubits, *Phys. Rev. Lett.* **100**, 200502 (2008).
- [68] D. Le Sage, L. M. Pham, N. Bar-Gill, C. Belthangady, M. D. Lukin, A. Yacoby, and R. L. Walsworth, Efficient photon detection from

color centers in a diamond optical waveguide, *Phys. Rev. B* **85**, 121202 (2012).

- [69] R. Kubo, Generalized cumulant expansion method, *Journal of the Physical Society of Japan* **17**, 1100 (1962).

## V. SUPPLEMENTARY MATERIALS

### A. Heuristic argument on added noise

In this section, we adapt Caves' derivation of the quantum limit on the added noise of a bosonic linear amplifier [17] to the phase-preserving spin amplifier considered in this work. We start by writing down a minimal description (in terms of Heisenberg equations of motion) of a spin amplifier that amplifies any polarization transverse to the  $z$  direction. The amplification process translates an input state (as encoded in the initial-time  $t = 0$  collective spin operators  $\hat{S}_\alpha \equiv \hat{S}_\alpha(0)$  for  $\alpha \in \{x, y, z\}$ ), to an output state (similarly encoded in the final time  $t = T$  Heisenberg-picture spin operators  $\hat{S}_\alpha(T) \equiv \hat{T}_\alpha$ ). Assuming linear amplification dynamics suggests writing the the solution of the Heisenberg equations of motion in the form:

$$\hat{T}_x = G(T)\hat{S}_x + \hat{F}_x, \quad (58)$$

$$\hat{T}_y = G(T)\hat{S}_y + \hat{F}_y. \quad (59)$$

The first term in each equation captures the linear amplification dynamics, with  $G(T)$  denoting the gain. The remaining Hermitian operators  $\hat{F}_\alpha$  describe all additional terms arising from solving the Heisenberg equations. Note that at this stage, we do not make any assumptions about the dynamics of  $\hat{S}_z$  and the value of  $\hat{S}_z(T) \equiv \hat{T}_z$ .

We next *assume* that the average values of the final-time spin operators are fully described by the linear gain terms (e.g. as is seen in our system for initial states with small transverse polarizations). As such, the  $\hat{F}_\alpha$  can be viewed as zero-mean operators that describe added noise associated with the amplification dynamics. We further assume that these noise operators are uncorrelated with the initial spin state, i.e.  $\langle \hat{S}_\alpha \hat{F}_\beta \rangle = 0$  and  $[\hat{S}_\alpha, \hat{F}_\beta] = 0$ . In reality, the  $\hat{F}_\alpha$  also describe the nonlinear response of our system; we are implicitly assuming that the initial state of our system lets us safely ignore such terms (i.e. the initial transverse polarization is small).

With these assumptions in hand, we can now construct a bound on the size of the added noise. We first use the fact that the final-time spin operators must obey canonical spin commutation relations, and hence we must have  $[\hat{T}_x, \hat{T}_y] = i\hat{T}_z$ . This results

in the constraint

$$\hat{T}_z = G^2(T)\hat{S}_z - i[\hat{F}_x, \hat{F}_y]. \quad (60)$$

The fluctuations in the final-time transverse spin operators are given by:

$$\begin{aligned} (\Delta T_{x,y})^2 &\equiv \langle \hat{T}_{x,y}^2 \rangle - \langle \hat{T}_{x,y} \rangle^2 \\ &= G^2(T)(\Delta S_{x,y})^2 + \langle \hat{F}_{x,y}^2 \rangle. \end{aligned} \quad (61)$$

Since the amplifier acts identically on the  $x$  and  $y$  components,  $\langle \hat{F}_x^2 \rangle$  and  $\langle \hat{F}_y^2 \rangle$  are identical and we can write

$$\begin{aligned} \langle \hat{F}_{x,y}^2 \rangle &= \frac{1}{4} \langle \{\hat{F}_+, \hat{F}_-\} \rangle \geq \frac{1}{4} |\langle [\hat{F}_+, \hat{F}_-] \rangle| \\ &= \frac{1}{2} |\langle [\hat{F}_x, \hat{F}_y] \rangle| = \frac{1}{2} |G^2(T)\langle \hat{S}_z \rangle - \langle \hat{T}_z \rangle|, \end{aligned} \quad (62)$$

where we defined  $\hat{F}_\pm = \hat{F}_x \pm i\hat{F}_y$  and used Eq. (60) in the last step. Using  $|\partial_\phi \langle \hat{T}_{x,y} \rangle| = G(T)|\partial_\phi \langle \hat{S}_{x,y} \rangle|$ , we thus find

$$\begin{aligned} \frac{(\Delta T_{x,y})^2}{|\partial_\phi \langle \hat{T}_{x,y} \rangle|^2} &\geq \frac{(\Delta S_{x,y})^2}{|\partial_\phi \langle \hat{S}_{x,y} \rangle|^2} \\ &+ \frac{1}{2G^2(T)} \frac{|G^2(T)\langle \hat{S}_z \rangle - \langle \hat{T}_z \rangle|}{|\partial_\phi \langle \hat{S}_{x,y} \rangle|^2}. \end{aligned} \quad (63)$$

In our specific spin amplification protocol, we start with a CSS close to a maximally polarized state, i.e.  $\langle \hat{S}_z \rangle = 2(\Delta S_{x,y})^2 = N/2$ , and we interrupt the amplification dynamics at the time  $T = t_{\max}$  when the condition  $\langle \hat{T}_z \rangle = 1/2$  holds. This yields

$$\frac{(\Delta T_{x,y})^2}{|\partial_\phi \langle \hat{T}_{x,y} \rangle|^2} \geq \frac{1}{N} \left[ 2 - \frac{1}{G^2(T)N} \right], \quad (64)$$

i.e. the spin amplification process doubles the input spin-projection noise in the large- $N$  limit.

Note that this argument is *not* a strict theoretical lower bound on the noise that is added during the amplification step. Instead, it is a heuristic argument that helps one to develop a sense how much added noise can be expected due to amplification. Even though our amplification scheme is conceptually very simple, we numerically find that it does not saturate the prediction of this heuristic argument (see Figs. 3(b) of the main text and Fig. 12 below). Hence, an interesting question for future research is to refine this argument to see if the actual lower bound on the added noise in the large- $N$  limit is larger than predicted here.

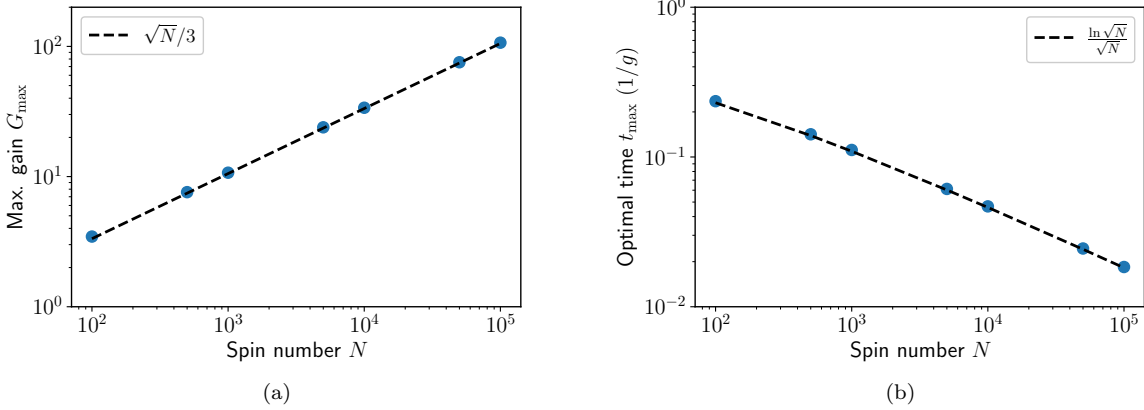


FIG. 10. Mean-field theory analysis of the coherent amplification protocol (i.e. in the limit of an undamped cavity). Scaling of (a) the maximum gain  $G_{\max}$  and (b) the corresponding time  $t_{\max}$  as a function of spin number  $N$ . Results have been obtained by numerical solution of the MFT equations (66) to (77). Blue dots correspond to simulation data, while dashed black lines show the respective scaling behavior.

### B. Mean-field theory in the limit of an undamped cavity

As discussed in the main text, amplification can also be achieved in a regime where the cavity degree of freedom cannot be eliminated adiabatically, i.e.  $\sqrt{N}g \gg \kappa$ . In this section, we use MFT to analyze the coherent limit of Eq. (25) of the main text (i.e.  $\kappa \rightarrow 0$ ). MFT lets us explore substantially larger system sizes than direct numerical simulation of the Schrödinger equation (which were used to generate the data shown in Fig. 8 of the main text). We consider the resonant ( $\omega_{\text{cav}} = \omega$ ) Tavis-Cummings Hamiltonian (29) of the main text, which reads in a frame rotating at the cavity frequency

$$\hat{H}_{\text{TC}} = g \left( \hat{a}^\dagger \hat{S}_- + \hat{a} \hat{S}_+ \right), \quad (65)$$

and we consider a separable initial state consisting of the cavity mode in a vacuum, and the spins maximally polarized in a state  $e^{i\phi \hat{S}_x} |\uparrow \dots \uparrow\rangle$ . Using a second-order cumulant expansion [69], we can derive a closed set of equations of motion (EOMs) for the spin-cavity system. Introducing the cavity quadrature operators  $\hat{Q} = (\hat{a}^\dagger + \hat{a})/\sqrt{2}$ , and  $\hat{P} = i(\hat{a}^\dagger - \hat{a})/\sqrt{2}$  as well as the notation  $Q = \langle \hat{Q} \rangle$ ,  $C_{Px} = \langle (\hat{P} \hat{S}_x + \hat{S}_x \hat{P}) \rangle / 2 - \langle \hat{P} \rangle \langle \hat{S}_x \rangle$ , etc., we can read-

ily write down the set of MFT equations of motion:

$$\dot{Q} = -\sqrt{2}g S_y, \quad (66)$$

$$\dot{S}_y = -\sqrt{2}g (C_{Qz} + S_z Q), \quad (67)$$

$$\dot{S}_z = +\sqrt{2}g (C_{Px} + C_{Qy} + S_y Q), \quad (68)$$

$$\dot{C}_{QQ} = -2\sqrt{2}g C_{Qy}, \quad (69)$$

$$\dot{C}_{Qy} = -\sqrt{2}g (C_{Qz} Q + C_{QQ} S_z + C_{yy}), \quad (70)$$

$$\dot{C}_{Qz} = +\sqrt{2}g (C_{Qy} Q + C_{QQ} S_y - C_{yz}), \quad (71)$$

$$\dot{C}_{PP} = -2\sqrt{2}g C_{Px}, \quad (72)$$

$$\dot{C}_{Px} = -\sqrt{2}g (C_{PP} S_z + C_{xx}), \quad (73)$$

$$\dot{C}_{xx} = -2\sqrt{2}g C_{Px} S_z, \quad (74)$$

$$\dot{C}_{yy} = -2\sqrt{2}g (C_{yz} Q + C_{Qy} S_z), \quad (75)$$

$$\dot{C}_{yz} = \sqrt{2}g [C_{Qy} S_y + (C_{yy} - C_{zz}) Q - C_{Qz} S_z], \quad (76)$$

$$\dot{C}_{zz} = 2\sqrt{2}g (C_{yz} Q + C_{Qz} S_y). \quad (77)$$

All expectation values (within the second-order cumulant expansion approximation) which are not explicitly shown above have only a trivial evolution, i.e. they remain zero. As an aside, we note that there are two constraints that are also satisfied by our system. The first one is total-angular-momentum conservation, which lets us write

$$S_x^2 + C_{xx} + S_y^2 + C_{yy} + S_z^2 + C_{zz} = \frac{N}{2} \left( \frac{N}{2} + 1 \right), \quad (78)$$

and the second one is conservation of the total excitation number, which yields

$$\frac{1}{2}(C_{QQ} + Q^2 + C_{PP} + P^2 - 1) + S_z = \frac{N}{2}. \quad (79)$$

Either (or both) of the above constraints could be used to further reduce the full set of EOMs shown above.

### 1. Scaling of the gain

Solving the system of equations (66) to (77) numerically, we can study the scaling of the maximum gain  $G_{\max}$  as well as the corresponding time scale  $t_{\max}$  for systems with very large spin number  $N$ , a regime which is inaccessible by numerical integration of the Schrödinger equation. Figure 10(a) shows the scaling of  $G_{\max}$ , while panel (b) displays the corresponding time  $t_{\max}$  required to reach the optimal gain value, both as a function of spin number  $N$ . We observe scaling behavior that very closely resembles the one observed for smaller- $N$  Schrödinger-equation simulations shown in Fig. 8 of the main text. Like in the dissipative version of our amplification protocol, the gain scales  $\propto \sqrt{N}$ , while  $t_{\max}$  has a parametrically slower  $N$ -scaling,  $t_{\max} \propto \ln \sqrt{N} / \sqrt{N}$ .

### 2. Semi-classical theory

Following work in [53], one might hope that much of the core physics or the amplification in the coherent limit of our amplification protocol could be captured by a semiclassical approximation, where all fluctuations (i.e. the covariances) are neglected. Such a case would let us simplify the set of Eqs. (66) to (77) to

$$\dot{Q} = -\sqrt{2}gS_y, \quad (80)$$

$$\dot{S}_y = -\sqrt{2}gS_zQ, \quad (81)$$

$$\dot{S}_z = +\sqrt{2}gS_yQ, \quad (82)$$

which, using Eq. (79) could be further reduced to

$$\dot{Q} = -\sqrt{2}gS_y, \quad (83)$$

$$\dot{S}_y = -\sqrt{2}g \left( \frac{N}{2} - \frac{1}{2}(Q^2 - 1) \right) Q. \quad (84)$$

These semiclassical equations indeed predict that  $S_y$  will grow at short time. However, solving Eqs. (83) and (84) numerically, one finds that  $S_y$  increases monotonically over a time scale much longer than  $t_{\max}$  obtained from MFT, see Fig. 11. Therefore, it is clear that one must include the effects of fluctuations to properly describe the amplification physics in the coherent  $\kappa \rightarrow 0$  limit.

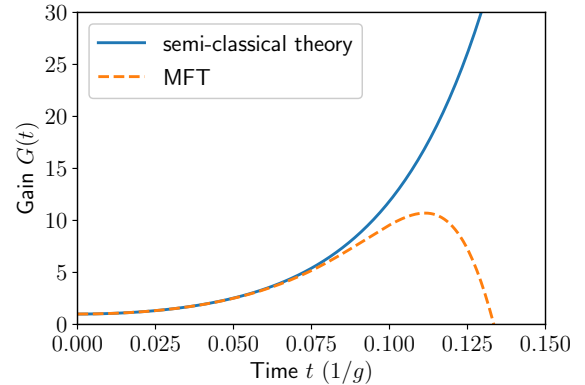


FIG. 11. Comparison between mean-field theory and a semiclassical approximation of the amplification dynamics. Gain as a function of time obtained from MFT (given by Eqs. (66) to (77)) as well as a semiclassical approximation (given by Eqs. (83) to (84)) for  $N = 1000$ . The semiclassical approximation cannot be used to properly describe the evolution of the cavity-spin system.

### C. Added noise $\sigma_{\text{add}}^2$ in the limit of an undamped cavity

Above, we gave a heuristic argument (assuming linear amplification dynamics) which showed that the added noise  $\sigma_{\text{add}}^2$  (defined in Eq. (13) of the main text), should approximately follow the relation

$$\sigma_{\text{add}}^2 \geq 1 - \frac{1}{G_{\max}^2 N} \quad (85)$$

in the limit of large spin number  $N$ . For dissipative amplification, we found numerically that the added noise stays close to this heuristic expectation and tends to  $\sigma_{\text{add}}^2 \approx 1.3$  in the large- $N$  limit (see Fig. 3(b) of the main text). Here, we show that similar behavior is also present in the case of purely coherent evolution, where  $\kappa \rightarrow 0$ . Specifically, Fig. 12 shows  $\sigma_{\text{add}}^2$  as a function of spin number  $N$ . Black dots correspond to data obtained from solving the Schrödinger equation numerically, while the dashed blue line indicates  $1 - 1/G_{\max}^2 N$ . Curiously, we see similar behavior to the dissipative case and observe  $\sigma_{\text{add}}^2 \lesssim 1.3$  in the large- $N$  limit. Consequently, our amplification protocol could also be useful in the coherent limit if the readout noise is not extremely large and one cares about approaching the SQL.

### D. OAT amplification with single-spin dissipation using mean-field theory

In the main text we showed that the performance of the OAT amplification protocol is particularly

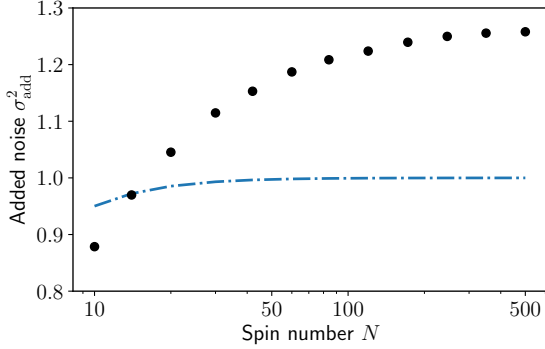


FIG. 12. Added noise  $\sigma_{\text{add}}^2$  in the coherent spin-amplification protocol, calculated by numerical integration of the Schrödinger equation using the resonant Tavis-Cummings Hamiltonian given in Eq. (29) of the main text with  $\omega_{\text{cav}} = \omega$ . The quantity  $\sigma_{\text{add}}^2$  at the optimal evolution time  $t_{\text{max}}$  (data points) is close to the amount of noise  $1 - 1/G_{\text{max}}^2 N$  that is expected based on a heuristic argument valid in the limit  $N \gg 1$  (dashed-dotted line).

sensitive to noise, both collective decay (governed by the cavity relaxation rate  $\kappa$ ) as well as single-spin dephasing and single-spin relaxation (governed by the rates  $\gamma_\phi$  and  $\gamma_{\text{rel}}$  respectively). Here, we present additional results obtained using MFT simulations, which explore this effect in more detail.

As discussed in the main text, collective decay generates a large background that needs to be subtracted to extract the amplified signal. Therefore, we consider the gain  $G_{\text{sub}}^{\text{OAT}}(t)$  defined in Eq. (36) of the main text, which is the signal after background subtraction,  $\delta\langle\hat{S}_y(t)\rangle = \langle\hat{S}_y(t, \phi)\rangle - \langle\hat{S}_y(t, 0)\rangle$ , normalized to the initial signal  $\langle\hat{S}_z\rangle = N\phi/2$ . Single-spin decay decreases the gain over time and therefore limits the maximum possible amplification time. To determine the maximum gain, one thus has to optimize both the detuning (which determines the ratio between the OAT strength  $\chi$  and the collective decay rate  $\Gamma$ , see main text), and the amplification time  $t_{\text{max}}$ . The result of this optimization is shown in Fig. 13, where we compare  $G_{\text{sub}}^{\text{OAT}}(t)$  to its ideal value obtained in the limit  $\eta_k \rightarrow \infty$  (i.e. no local dissipation). The gain in this limit is equivalent to the gain in the absence of any dissipation, since the condition  $\Delta_{\text{opt}} \gg \kappa$  holds, i.e. collective dissipation is strongly suppressed. Similar to Fig. 9(a) of the main text, we evaluate the maximum gain at the time  $t_{\text{max}} = \tau_1$  of the first peak of  $G_{\text{sub}}^{\text{OAT}}(t)$ . Figures 13(a) and (b) show data for single-spin dephasing and single-spin relaxation, respectively, and the insets show the corresponding values of the optimal spin-cavity detuning  $\Delta_{\text{opt}}$ . In both scenarios, very high *single-spin* cooperativities are required to result significant gain: one needs  $\eta_\phi \gg \sqrt{N}$  and  $\eta_{\text{rel}} \gg N^{0.9}$ .



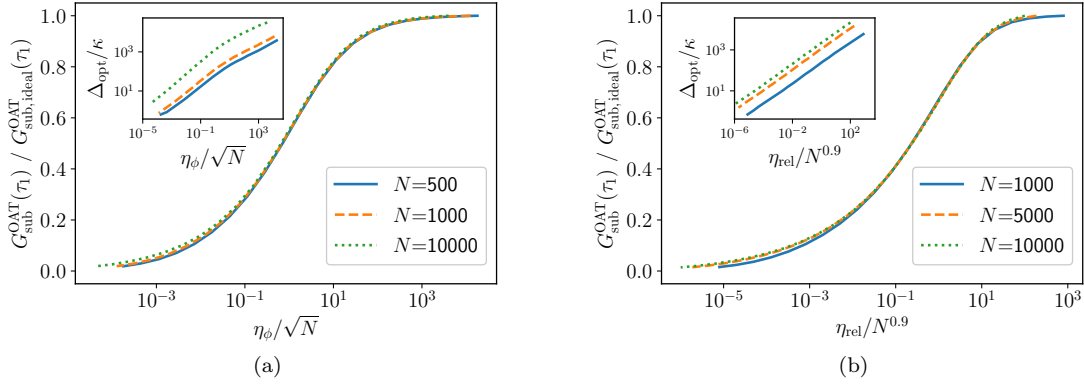


FIG. 13. Performance of the OAT spin amplification protocol proposed in Ref. [19] in the presence of (a) single-spin dephasing and (b) single-spin relaxation. Each plot shows the optimal gain  $G_{\text{sub}}^{\text{OAT}}(t)$  after background subtraction (evaluated at the time  $\tau_1$  of the first peak) as a function of the single-spin cooperativity  $\eta_k$  (with  $k = \{\phi, \text{rel}\}$ ), normalized to the gain calculated in the limit  $\eta_k \rightarrow \infty$ . Simulations were done using MFT for  $N = 1000, 5000$ , and  $10000$  spins, and the spin-cavity detuning was optimized for each value of  $\eta_k$  (see insets). These plots suggest that, to achieve significant performance, the *single-spin* cooperativity must be substantially large and satisfy  $\eta_\phi \gg \sqrt{N}$  and  $\eta_{\text{rel}} \gg N^{0.9}$ .